MODELING, CONTROL AND SOLID STATE INFRARED ARRAY SENSING OF TEMPERATURE DISTRIBUTION DURING GAS METAL ARC WELDING

REPORT NO. UM-MEAM-88-03

Taikdong Cho

Graduate Student

Elijah Kannatey-Asibu

Associate Professor

Department of Mechanical Engineering

and Applied Mechanics

The University of Michigan

Ann Arbor, MI 48109

Final Report To:

Welding Research Council

345 East 47th Street

New York, NY 10017

ensp

UNR1160

ABSTRACT

Noncontact sensors are essential for monitoring and control of weld temperatures to improve quality. Recent developments in solid state infrared array detection open the avenue for accomplishing such a feat. This report presents an investigation unto its application to an arc welding process. Through an analysis of infrared radiation and radiometry, a laboratory built infrared array detector was calibrated and shown to be highly suited for general application to welding. Emissivity variation for the surface conditions normally encountered were measured and found negligible. Background arc and weld pool effects or interference on the detector were analysed and techniques developed for eliminating them where possible. The infrared detector measurements were also found to correlate remarkably well with thermocouple outputs especially when the thermal response was not rapid.

CONTENTS

Abstract i

List of Tables iii

Figure Captions iv

Nomenclature v

I. Introduction 1

II. Infrared Detector and Calibration of the System 4

II.1 Brief Review of the Radiometric Calibration..... 4

II.2 Infrared Camera Design 7

II.3 Measurement of Infrared Detector Characteristics 12

III. The Infrared Array Responses 19

III.1 Temperature Calibration with Indirect Heat Source 19

III.2 Temperature Calibration during Welding 21

III.3 Estimation of Interference from Arc Area 24

IV. Conclusions 29

References 32

Appendix: Spectrum of the Radiation from a Welding Arc 35

Figures 41

List of Tables

Table 1: ZnSe Refractive Index vs. Wavelength 9

Table 2: KBr Refractive Index vs. Wavelength 10

Table 3: I.R. Detector Internal Noise and Resistance 13

Table 4: Responsivity of Infrared Detector Elements 16

Table 5: Ionization Potentials for Various Elements 38

Table 6: Composition of Plasma-Mig Welding Arc 39

Figure Captions

Fig. 1 Radiation from surface element to surrounding.

Fig. 2 Infrared detecting system.

Fig. 3a Calibration chart for optical filter 1: Germanium.

Fig. 3b Calibration chart for optical filter 2: Silicon.

Fig. 4 Detector noise with optical filter 2.

Figs. 5 to 7 Response of infrared detector without collecting lens.

Figs. 8 to 10 Response of infrared detector with collecting lens.

Fig. 11 Comparison of infrared detector and the thermocouple output.

Fig. 12 A typical plot of infrared and thermocouple responses.

Fig. 13 Plots of temperature calibrated infrared signals vs. thermocouple measured values.

Fig. 14 Plots showing emissivity effect on infrared detector signals.

Fig. 15 Infrared and thermocouple signals during welding with optical.

Fig. 16 Radiant intensity through optical elements.

Fig. 17 3 measurement plots of infrared detector without optical filter.

Fig. 18 Interference mechanisms.

Fig. 19 Reflected radiation in the signal plot.

Fig. 20 Interference from system resolution.

Fig. 21 Plot of interference test data.

Fig. 22 Spectrum of 100 amp argon arc between 3700 and 4900 Å.

Fig. 23 Vapor pressure vs. temperature of metals.

NOMENCLATURE

A	Atom in initial energy state
A_c	Aperture area of the collector
A_s	Area of the radiation source
A_d	Detector sensing area
A_λ	Transition probability
A^*	Atom in excited state
c	Speed of light (2.998x10^8 m/sec)
E	Arc voltage
E_h, E_b	Lower and upper energy levels of Atom
e	Electric charge of an electron (1.602x10^{-19} Coulomb)
f	Focal length of the collector
g	Statistical weight in spectrum analysis
h	Planck's constant (6.6256x10^{-34} J sec)
I	Welding current
I_λ	Spectral intensity
L	Sterance or radiance
L_{av}	Average sterance
L_s	Sterance on the source
M	Areance or radiant existance
m	Magnification ratio
m_e	Mass of the electron (9.108x10^{-31} Kg)

$n(T)$	Atom density in arc at temperature T
p	Pressure
R	Responsivity
T_p	Throughput (projected area times solid angle)
u	Object distance
V	Detector output voltage
V^*	Internal energy change for an excited atom
$Z(T)$	Partition function
α	Thermal diffusivity
α_i	Degree of first ionization of the atom
γ_r	Reflectance
γ_a	Absorptance
γ_t	Transmittance
ϵ	Emissivity
θ_1, θ_2	Source temperature and ambient temperature
κ	Boltzmann constant (1.38×10^{-23} J/K)
λ	Wavelength of particle
ν	Frequency of particle in atom
Φ	Flux or radiant power
Φ_a	Absorbed flux
Φ_c	Total flux on collector
Φ_r	Reflected flux
Φ_t	Transmitted flux

σ	Stefan-Boltzmann constant (5.67 x $10^{-8} w/m^2 K^4$)
ω	Solid angle
ω_s	Solid angle of the collector

I. INTRODUCTION

Automation of manufacturing processes has emerged as one of the most important research areas in the last few decades. The basic issues involved include modeling, monitoring, and control of the process. The complexity of manufacturing processes has limited the application of advanced control theory to the manufacturing industry. The other limitation is the shortage of reliable sensors.

Recent trends towards robotic welding seems inevitable to achieve high and uniform quality as well as increasing productivity. To accomplish this objective, it is essential to study the fundamental behavior of the welding process. Welding is a complex multi-input, multi-output process. To control the welding process adequately, all the parameters need to be considered. Some of them would be regulated in-process, some would be preset before welding, and some should be manipulated in both ways through the interrelationship between them. The primary input variables are the machine input parameters such as arc voltage or current, wire feed speed and welding speed. The primary output variables are usually not measurable in-process, and include penetration, hardness, and bead defects. Therefore in-process control to improve weld quality requires indirect methods that involves controlling measurable intermediate parameters which can then be related to the desired final output based on theory or experiment.

The temperature distribution is one such measurable intermediate output. Since welding involves localized melting with the rest of the surrounding weldment at a relatively low temperature, the temperature positions of interest are

close to the pool. The temperature distribution is very sensitive to changes in the pool conditions, and helps decide the input variables. Once the optimum conditions are obtained, they can be controlled through the feedback control scheme to obtain uniform quality in the weld bead. To achieve this goal, a critical problem has been the development of a suitable sensor for monitoring the system. It should faithfully follow the torch and maintain constant distance without disturbing the process. Two types of sensors commonly used for surface temperature measurement are infrared detectors and thermocouples. The infrared detector is more suited to in-process monitoring since it is a noncontact sensor.

Research on infrared sensors and their application to special areas such as defense, medical science, etc., has been enormous, and is still very active. Moreover, new design concepts and advanced integrated circuit manufacturing technology have improved the quality, and simplified the signal processing elements. The solid state infrared array detector technology holds promise over the scanning system. However, application of the infrared array sensor to industry, especially welding process control, is still in its infancy. The objective of this research is application of the array infrared detector to welding process control, and development of a feedback control algorithm by first modeling the weldment thermal response. A substantial effort has been made to evaluate the 7-element array infrared detector under the severe conditions of the welding process. An optical system has been designed, using commercial infrared lenses and optical filters. The infrared camera was then calibrated using a 500° K blackbody.

This report discusses the characteristics of the infrared array sensor being develped for low cost weld process monitoring. Basic radiometric theory is the starting point for the infrared sensor because it deals with the calibration of radiation from the temperature source to the sensor. The characteristics of the infrared detector was tested primarily using an ordinary heated surface. In this case, the process is usually ideal without any interference, unlike actual welding. Interference during actual welding was also measured and its effect on the signal considered. Some of the interference mechanisms could be eliminated using suitable shielding, others were expected to be improved with a better infrared device, and still others were found to be inevitable in the vicinity of the welding arc.

The literature on arc spectra was studied along with the theory of quantum physics. Based on this background, efforts were made to reduce the arc effect. Longwave pass optical filters were applied for this purpose. However, their implementation in welding was not very successful because it reduced the amplitude of the signal from the temperature field. For reference, K-type thermocouples were used to confirm the reliability of the infrared detector.

II. INFRARED DETECTOR AND CALIBRATION OF THE SYSTEM

The infrared sensor was supplied by the Solid State Lab in the Department of Electrical Engineering and Computer Science of the University of Michigan at Ann Arbor where it was developed and fabricated as a prototype silicon thermopile array [1]. The array is based on polysilicon-gold thermopiles supported on $1.3\mu m$ thick dielectric diaphragm windows composed of 3 layers that include a 300 nm thick thermal silicon dioxide, 200 nm thick silicon nitride, and another 800 nm thick silicon dioxide. Each thermopile element has 40 polysilicon-gold thermocouples, and the size of the dielectric diaphragm window is 400 x 800 μm. Due to the lack of specific characteristic data, it was calibrated in the Intelligent Welding Systems Lab to evaluate some of the important parameters.

II.1 Brief Review of the Radiometric Calibration [2]

The measurement of radiation is always related to the concept of flux, which propagates and is spatially distributed. Because radiation is a function of direction and distance, these two variables need to be carefully considered to get an accurate value of input power incident on the detector through the optical system. Using the concept of solid angle for convenience, the average sterance L_{av} is defined as

$$L_{av} = \frac{d\Phi}{dT_p} \tag{1}$$

where Φ is the total flux, T_p is the product of the projected area and solid angle, which is sometimes called throughput [1]. The areance M is defined as

$$M = \frac{d\Phi}{dA_s} \tag{2}$$

where A_s is the area of the radiation source. From the Stefan-Boltzmann law, M for a gray body of temperature θ_1 with an ambient temperature θ_2 in absolute scale is

$$M = \epsilon\sigma(\theta_1^4 - \theta_2^4) \tag{3}$$

where ϵ is emissivity, and σ is the Stefan-Boltzmann constant. From the elemental radiating surface ΔA_s, the flux radiates in all directions. From Eq. (1), the amount of flux falling on the elemental area ΔA_d of the unit radius hemisphere is

$$\begin{aligned} d\Phi &= L_s\, dT \\ &= L_s\, \Delta A_s\, cos\varphi\, d\omega \end{aligned} \tag{4}$$

where L_s is sterance of the source [2], and $d\omega$ solid angle of elemental area ΔA_d. Thus the total flux from the element of radiating surface could be obtained by integrating Eq. (4) over the hemispherical surface A. Then

$$\begin{aligned} \Phi &= L_s \Delta A_s \int_A cos\varphi d\omega \\ &= L_s \Delta A_s \int_A cos\varphi \frac{dA_d}{r^2} \\ &= L_s \Delta A_s \int_0^{\frac{\pi}{2}} cos\varphi \frac{(2\pi r d\varphi)(r sin\varphi)}{r^2} \\ &= L_s \Delta A_s \pi \end{aligned} \tag{5}$$

[1] This is the combined parameter of all the geometric variables of source and measurement. $\Delta T_p \equiv \Delta A_1 \Delta\Omega_1 = \Delta A_2 \Delta\Omega_2$ because $\Delta A_1 cos\psi(\Delta A_2 cos\phi)/s^2 = \Delta A_2 cos\phi(\Delta A_1 cos\psi)/s^2$ as shown Fig.1b.

[2] Flux per unit throughput.

where r is the radius of the hemisphere. On the other hand, the flux from the area ΔA_s is also defined as

$$\Phi = M\Delta A_s \tag{6}$$

Therefore, from equations (3),(5) and (6) the radiation flux from a unit source area per solid angle, or sterance, becomes

$$L_s = \frac{\epsilon\sigma({\theta_1}^4 - {\theta_2}^4)}{\pi} \tag{7}$$

The infrared monitoring system is schematically represented in Fig. 2 where the optical infrared detector is located at the focal plane of the infrared camera. From equation (4), the total flux incident on the collecting lens Φ_c then becomes

$$\Phi_c = \int_{A_s}\int_{\omega_s} L_s cos\varphi d\omega_s dA_s \tag{8}$$

If the sterance L_s is assumed uniform over the area A_s, and the aperture of the collector is relatively small compared to the object distance u, then since the solid angle of the collector ω_s is obtained from the aperture area of the collector A_c and object distance u, equation (8) can be approximated as

$$\begin{aligned} \Phi_c &\approx L_s A_s \omega_s \\ &\approx L_s A_s \frac{A_c}{u^2} \end{aligned} \tag{9}$$

From equations (7) and (9), the total radiation flux from the source of temperature θ_1 becomes approximately

$$\Phi \approx \frac{\epsilon\sigma({\theta_1}^4 - {\theta_2}^4)}{\pi} A_s \frac{A_c}{u^2} \tag{10}$$

when the ambient temperature is θ_2. This amount of radiation flux flows into the detector sensing area A_d through the collecting lens if the energy loss during passage through the optical elements is neglected. In the case of an extended radiation source, the object area can be expressed in terms of the detector area and magnification ratio of the optical system as

$$A_s = \frac{A_d}{m^2} \tag{11}$$

where m is the magnification ratio[3]. Finally the total radiant power Φ_p incident on the detector window becomes

$$\Phi_p = \frac{\epsilon\sigma(\theta_1^4 - \theta_2^4)}{\pi} \frac{A_d A_c}{(mu)^2} \tag{12}$$

The actual energy incident on the thermopile detector can only be obtained after considering losses through the optical elements between the source and detector. The polysilicon-gold thermopile detector output is voltage and is approximately linear with the input radiant flux.

II.2 Infrared Camera Design

The welding temperature range that the infrared detector measures varies from room temperature up to near the melting temperature of the weldment. For steel, this is about 1800^0 K. The most important thing to be considered then is the change in the optical characteristics of the system elements. It should also operate in the harsh welding enviroment with high intensity radiation from both the arc and weld pool, spatter, and harmful fumes which leave deposits on

[3]Magnification ratio $m = \frac{f}{u-f}$ for a thin lens with a focal length f.

contacting surfaces. Moreover, it should work properly in spite of the sporadically unstable state of the strong arc radiation. Effective application thus requires the selection of optical elements that can accomodate the variety of welding conditions. A detailed discussion on the specification of the optical elements follows.

Infrared Lens

From the characteristics of infrared radiation from welding, several requirements were considered essential in selecting the infrared lens. They include

1. Temperature range to be measured
2. Severe welding environment
3. High temperature gradient in the immediate neighborhood of the weld bead

Primary considerations are

1. Low refractive index material
2. Small variation of refractive index with wavelength
3. Wide wavelength range
4. Lens shape that permits high magnification
5. Resistance to thermal shock and moisture corrosion

A ZnSe f/2 meniscus type lens with 1.5 *inch* diameter and anti-reflection coating was considered most appropriate. The refractive index change of ZnSe is quite

Table 1: ZnSe Refractive Index vs. Wavelength [3]

$\lambda(\mu m)$	n	$\lambda(\mu m)$	n
2.75	2.44	15.0	2.37
5.00	2.43	16.0	2.36
7.50	2.42	16.9	2.35
9.50	2.41	17.8	2.34
11.0	2.40	18.5	2.33
12.5	2.39	19.3	2.32
13.5	2.38	20.0	2.31

small over a wide range of the optical wavelength. Also, the material is known to be strong enough to withstand the moisture or thermal shock. The optical characteristics of the material and data are shown in Table 1.

Protection Window

To protect the detector, a KBr window was used to cover the front opening of the detector package. KBr has a very wide range of optical wavelength with good transmittance. However, it is sensitive to moisture over a long exposure time. The material characteristics are listed in Table 2.

Table 2: KBr Refractive Index vs. Wavelength [3]

$\lambda(\mu m)$	n	$\lambda(\mu m)$	n
0.39	1.59	12.0	1.52
0.44	1.58	17.0	1.51
0.49	1.57	18.1	1.50
0.59	1.56	20.5	1.49
0.80	1.55	22.0	1.48
1.50	1.54	23.9	1.47
8.50	1.53	25.2	1.46

Optical Filter

Arc and weld pool interference can introduce significant error in the temperature measurement. The discussion in Appendix shows that the majority of the radiation argon gas arc emitted by an major radiation is in the wavelength range below 2.5 μm. The metal vapor in the welding arc that originates from the molten electrode and weldment radiates the same range of wavelength emission as argon but with less intensity. However, a significant portion of infrared radiation from the solid workpiece is of long wavelength. Thus, an optical filter can be used

to eliminate unwanted signals from the arc efficiently. With this filter, the net signal level decreases and the Stefan-Boltzmann equation is no longer applicable since the equation is effective over the entire range of continuous wavelength as a blackbody.

Two kinds of longwave pass filters were used. One was a germanium filter that transmits from 2.5 μm to 8.0 μm wavelength. The other was a silicon filter that transmits from 7.0 μm to 12.0 μm. The manufacturer's calibration charts are shown in Figs. 3a and 3b. But these optical filters were not adequate to completely filter out the arc noise. To further investigate this phenomenon, the detector was used to view the arc directly from the horizontal direction.

To prevent accidental damage to the detector, a longwave pass optical filter ($7\mu m \sim 12\mu m$) with a 3.5 mm diameter opening was installed in front of the lens. With a 19 inch object distance, only a noisy signal was obtained. The amplitude varied from element to element, but all had the same characteristics. The 1st and 3rd element outputs are shown in Fig. 4. The noise level reduced to that of the detector internal circuit when the arc stopped. When the opening area of the optical filter was increased to 11 mm diameter, the signal level did not change.

These results confirmed the filter function, but also opened up more serious questions. What is the source of the noise? What is the reason for the spikes and/or fluctuations of the infrared signal even through the same optical filter when the detector is focused at a point near the welding arc? These are issues

currently being addressed.

II.3 Measurement of Infrared Detector Characteristics

Calibration of the infrared detector under conditions similar to actual application is very important because all the measuring instruments have their own effective linear ranges beyond which their major characteristics deviate from linearity. This is especially important for the wide range of temperatures encountered in welding. When the detector is used as a sensor for control, its dynamic behaviour becomes critical. The time response of the sensor affects the overall characteristics of the control system.

The infrared detector used in this research was blackened to improve the absorptance. This unfortunately also increases the time response. The detector noise, responsivity and optical system response were measured. The responsivity of each element was obtained from RMS measurements at different distances with a $500^{o}K$ blackbody and also with a 5 mW He-Ne laser source. The optical system response was measured with the single ZnSe lens in place and was compared with the expected theoretical curve.

Noise

The signal output from the infrared detector is relatively small even under substantial radiation from a high temperature object. Thus the detector circuit noise can be relatively significant. The noise level of each element was measured

Table 3: I.R. Detector Internal Noise and Resistance

Channel	#1	#2	#3	#4	#5	#6	#7
Noise (μV)	4.7	4.7	4.7	4.6	4.5	4.5	4.5
Resistance(KΩ)	126.1	124.7	123.4	117.9	117.2	110.5	111.0

with the infrared detector completely enclosed in the camera, and external low frequency noise isolated through a careful arrangement of the system. The noise levels obtained as well as resistances of the 7 elements are illustrated in Table 3, and are very close to those obtained in [1].

The noise level of the infrared array detector may not be critical in itself because the absolute value is extremely small and their noise equivalent power (NEP) is around 2 x 10^{-7}, considering the responsivity of each element. The responsivities of the detector elements will be explained later. Even in the general purpose commercial infrared detector, this is a common NEP range [4]. If a suitable collecting lens is used in the camera system, the signal from a low temperature object could be measured accurately.

The frequency of the internal noise covers a wide band [1]. The results of Table 3 were obtained using a variable frequency low pass filter (Krohn-Hite, Model 3202) by changing the cut-off frequency and checking the RMS noise value. When a cutoff frequency of 20 Hz was applied, the RMS noise was reduced to less than

10 % of the noise value when it was measured without the filter.

Welding Noise

The detector noise is negligibly small under common radiation sources as explained above because the S/N ratio[4] is large enough in actual application. Thus the detector could be used without a noise filter. Despite that, the low frequency noise from the electric power lines was effectively shielded to ensure that the final signal output was free of noise. With the arc on, the noise was found to be severe as shown in Fig. 4, with a d.c. offset. This d.c. offset value is considered as the net signal. The first part is the noise with the arc on, and the second half represents the noise with the arc off. The experiment was done with the camera lens blocked to make sure there was no signal input into the detector. The summary of the noise phenomena is as follows:

1. The noise intensity of each detector element is different.

2. It decreases as the camera moves away from the arc area.

3. It does not change with different arc conditions.

4. A 20 Hz low pass filter almost completely eliminates the noise.

Comparing the radiations from the arc welding process and other objects, it was confirmed that there was no signal disturbance from any dynamic parts of the welding power supply when it was switched on without the arc. Thus the

[4]Signal to noise ratio.

arc is considered to be responsible for this noise. The high current through the arc and induced electromagnetic field around the arc seem to excite the detector element or line, and generate the noise.

Responsivity

One of the important parameters of the infrared detector, responsivity was calibrated using a $500^{o}K$ blackbody. The data obtained was analysed to determine if it agreed with radiation theory. When the source emits infrared radiation, the total flux incident on the detector thermopile window of area A_d is proportional to the inverse of the squared distance. This relation could be described by Eq. (9) with A_d replacing A_c since the equation was developed for the collector system. When the distance is more than 10 times the maximum transverse dimension of source area A_s or detector area A_d, the accuracy of the equation becomes about 99% [2].

The detector output after focusing on the $500^{o}K$ blackbody was amplified 60 dB. The measurement was repeated, changing the object distance. Plotting the measured data on a log-log scale, Figs. 5 to 7, showed a linear trend. This indicates that the detector element responses followed radiometric theory.

The object distance was limited between 2 *cm* and 7 *cm* to get appropriate signal level without the lens. From these results, the responsivity of each element was obtained as follows. When the collecting lens is not used, Eq. (10) becomes

$$\Phi = \frac{\epsilon\sigma(\theta_1{}^4 - \theta_2{}^4)}{\pi} A_s \frac{A_d}{u^2} \tag{13}$$

Table 4: **Responsivity of Infrared Detector Elements**

Channel	#1	#2	#3	#4	#5	#6	#7
Responsivity (V/W)	22.2	24.7	22.2	19.9	20.7	19.9	17.1

and the I.R. detector output is proportional to the total radiation flux incident on the detector thermopile window. Thus the voltage output V of a detector will be

$$V = R\Phi \tag{14}$$

where R is the responsivity of the detector, Φ the flux incident on it. A blackbody has a unit emissivity at a known temperature θ_1. Also, the room temperature θ_2 and other dimensions of the detector are known. The responsivity R was then obtained from a log-log plot of the measured data after least squares curve fitting of the plot. From Eqs. (13) and (14), we have

$$\log V = \log RC - 2 \log u \tag{15}$$

where u is the object distance from detector to target, and C is given by

$$C = \frac{\epsilon\sigma(\theta_1^4 - \theta_2^4)}{\pi} A_s A_d$$

The responsivity was then obtained from the intercept of the log-log plot with the signal axis, and is shown in Table 4.

The signals of all elements were measured at their maximum output by mov-

ing the detector across the optical axis at a fixed distance. Thus the calibration conditions of each element was the same. But the responsivity value for channel #7 was much lower than those for other elements. Other data such as the resistance of the thermopile circuit and noise were similar with the other 6 elements. The responsivity data obtained applies to a blackened detector with a KBr[5] protection window mounted.

I.R. Detector Response with Collecting Lens

The collecting element is necessary to get a higher signal output and a more precise point sensing. As described in the preceding section, a collecting lens with a much larger receiving area than the detector increases the solid angle, and thus the incident power. If the target is an expanded source and all the radiant flux through the collecting lens makes an image on the detector surface, then Eq. (12) indicates that the signal increases as the object distance increases. Physically, the trend continues until the image of the extended source becomes the same size as the detector thermopile area. Thus the limit is determined by the source size and magnification ratio of the camera system.

The experimental result showed this trend, and indirectly proved that the system responds adequately. The experimental condition was the same as the case without a lens. The $500^{o}K$ blackbody was also used for its constant temperature source, unit emissivity, and perhaps uniform temperature distribution over the outlet. Figs. 8 through 10 show the results for the first 6 elements even though

[5]Potasium bromide.

the amount of data is not enough to draw general conclusions. The theoretical response was calculated based on the responsivities obtained with a collecting lens as explained above.

III. THE INFRARED ARRAY RESPONSES

To check the detector capability over various thermal fields, several different issues were investigated experimentally.

III.1 Temperature Calibration with Indirect Heat Source

K-type (Chromel - Alumel) thermocouples were used and mounted in the steel plate. The sheath size of a 0.005 inch diameter bare wire was 0.025 inch. The infrared camera was focused at the point where the thermocouple was mounted, and the data obtained simultaneously from both as the specimen was heated or cooled. The purpose of this experiment was to check the following.

1. Repeatability of the detector output.

2. Reliability of the calibration procedure.

3. Dependence of emissivity on the surface conditions.

4. Estimation of interference from the arc area in actual welding.

Figs. 11 to 14 represent the results obtained. They show that infrared radiation signals corresponding to the thermocouple measured temperature were very close to each other during both heating and cooling. If the thermal field distribution at the sensing position is not significantly wide and the emissivity remains the same for the range, the infrared detector is expected to give the same results as the thermocouple. The infrared detector response curve is parabolic

in shape, Fig. 11, as expected from the calibration equation (Eq. 12). However, the calibrated temperatures from the thermocouple and infrared detectors showed some errors at the low and high end of the temperature range, Fig. 13. The reason for this difference may come from the large temperature gradient that exists around the high temperature area on the plate, as well as the time constant of the thermocouple. However, the relationship between the calibrated infrared radiation signal and the thermocouple data was quite linear, Fig. 13.

To get an idea about the effect of emissivity, the heating area was subjected to different treatments - clean, oxide, candle soot, and welding soot, Fig. 14. Above 550° C, the deviation begins to increase, but the difference is not as significant as was expected. Moreover, it is negligible at low temperatures, in contrast to other data [5].

Finally, this experiment could be used as a reference source for estimating the arc interference because it does not include the arc and weld pool effects which are inevitable during welding. If the same process is repeated in welding, the net signal difference could be attributed to interference because the difference originating from a temperature gradient change or surface condition may be small compared to the arc and weld pool interference.

In conclusion, the infrared detector has been confirmed to be reliable when the target is heated or cooled gently by an indirect heat source. However, it

needs further testing under the more severe arc welding conditions.

III.2 Temperature Calibration During Welding

The optical filter was considered a necessary component to reduce the arc interference effect. The filter was selected on basis of the wavelength characteristics of arc radiation. The argon arc is expected to emit short wavelength radiation primarily between ultra-violet and near infrared range[6]. Although metallic vapors exist inside an arc, their overall and spectral intensities do not exceed that of argon because their atom densities are much smaller than argon's, as explained in Appendix. Thus a longwave pass optical filter beyond the maximum expected wavelength from the argon arc was selected.

A disadvantage of the optical filter, however, is a reduction of the original signal intensity level. Also, the signal reduction rate is not uniform over a wide temperature range. Since only partial radiation energy is absorbed by the detector when a filter is used, the infrared detector signal cannot be interpreted using the Stefan-Boltzmann relation. Instead, Planck's formulation should be used.

In the actual welding process, the same procedure as discussed in the preceding section was applied, with an optical filter ($7\ \mu m \sim 12\ \mu m$), Fig. 15. A K-type thermocouple was planted on the focusing point of the infrared detector, and both signals were compared. The relation between the thermocouple and infrared signal with this filter appears to be almost linear, Fig. 16. An interesting

[6]Near infrared range: 0.75 μm to 2.5 μm wavelength

aspect is the response of the thermocouple during the heating period when the arc approaches and reaches its maximum temperature. The rapid heating with an 0.75 cm/sec welding speed made the thermocouple response lag. Thus the results appear to be much lower than that during the cooling period for the same temperature. In Fig. 15b, the upper trajectory is for the heating period and the lower one for the cooling period. The sharp peak response is regarded as an arc and weld pool effect as they pass near the focusing point.

When both measurements were analysed, the dynamic behaviour of the infrared detector could be neglected because its time response is much faster than the thermocouple's. The transient behaviour of the thermocouple could be approximated as a first order differential equation when it measured a rapidly changing temperature. However, the dynamic effect of the thermocouple would be negligible, and the actual value obtained if the measured temperature changes slowly as occurs during cooling of the HAZ after welding. Thus, the thermocouple readings while cooling are the true values, and the same for the infrared signals. Using the infrared data for both periods, the actual temperatures during the heating period could be estimated.

It was assumed that the thermocouple responded as a first order differential equation when it was inserted into a specimen. If the specimen temperature changes rapidly, the dynamic equation will be

$$\frac{d\theta}{dt} + \frac{1}{\tau}\theta = f(t) \tag{16}$$

where f(t) is related to the rate of temperature change in the test area. The function f(t) would be a measured temperature divided by the time constant when

the thermocouple was inserted into a fixed temperature body. Thus, f(t) was approximated to an time varying actual temperature devided by time constant of thermocouple. Using infrared data as a reference, the actual thermocouple values in heating period could be obtained from cooling period data .

This analysis confirmed not only the thermocouple time lag, but also the fast and sound response of the infrared detector with an optical filter in a rapidly varying thermal field as occurs in the welding system. The experimental and theoretical plots with and without the optical filter are shown in Fig. 17. The actual signal reduction in the infrared detector is exactly the same with the theoretical calculation.

III.3 Estimation of Interference from Arc Area

It has been found that the infrared detector works reliably well when there is no strong heat source near the sensing position. When the arc is close to the sensing position, it is evident that substantial interference occurs. It is also clear that the effect depends on the arc condition, sensing position, and focusing direction. A stable arc results in a more uniform interference, and an unstable one produces a spiky signal.

Most of the interference comes from the arc, weld pool, and just solidified bead. Usually, the weld pool is not limited to the arc contacting area, but is extended behind the welding electrode due to the welding speed and convection of the molten metal. The molten metal returns its latent heat to the back of the weld pool as it solidifies. Thus there exists a relatively high intensity infrared radiation from this portion of the bead.

Three types of interference signals appear to disturb the real signal. They include interference by stray radiation, interference by reflected radiation, and interfernce by the resolution of the infrared optical system.

Interference by Stray Radiation

The stray radiation comes from the area out of the field of view of the detector camera but reaches the detector by reflection inside the camera, on the wall. As shown in Table 2, the different wavelengths have different indices of refraction for the same optical material. Signals from untargeted locations can thus be focused

onto the detector, Fig. 18a. When the sensing point is outside the weld pool, this type of interference can be eliminated using a simple shield that cuts off the radiation from the arc area. The intense radiation can heat up the shield and emit parasitic radiation, but its intensity is expected to be negligible, and would not affect the measurement.

Interference by Reflected Radiation

If a radiant flux Φ is incident upon a body, it is split into three portions. One portion, Φ_r, is reflected by the body, another, Φ_a, is absorbed, while Φ_t is transmitted through the body. Thus

$$\begin{aligned} \Phi &= \Phi_r + \Phi_a + \Phi_t \\ 1 &= \gamma_r + \gamma_a + \gamma_t \end{aligned} \tag{17}$$

where γ_r is the reflectance, γ_a absorptance, and γ_t transmittance. But the metal used in welding is opaque to any radiant flux from the arc and weld pool, thus $\gamma_t = 0$. Hence

$$\gamma_r = 1 - \gamma_a \tag{18}$$

From Kirchoff's law, the emissivity ϵ and absorptance γ_a are the same, and the emissivity of a steel plate during welding is about 0.9 [5]. Thus, approximately 10 % of the direct radiation energy from the arc area to the target point is reflected and 90 % of it is absorbed. A portion of the reflected energy reaches the collecting lens and causes interference, Fig. 18b.

From the experimental results shown in Fig. 19, the reflected interference

appears just after the arc starts and remains as long as it exists. If the emissivity of the workpiece and the arc condition are kept relatively constant, the reflected interference would be an overall offset of the detector signal. It also depends on the distance from the arc area, but does appear to be more significant near the weld pool.

Interference by Resolution

The signal output of the detector is not limited to radiation from the point of interest but from a finite area that is decided by the optical relationship of the infrared camera. Normally, the infrared image is less sharp than the visible camera image for the same quality of optical elements due to the longer and wider band of wavelength characteristics. This is schematically illustrated in Fig. 20. The inner circle in Fig. 20a represents a theoretically decided object area, and the outer one corresponds to the actual area that affects the true image. Fig. 20b shows the radial intensity contributions to the camera output which focuses at the point $r = 0$. The total signal output is the integral of this intensity over the area around the target point.

When the target has no strong radiation source close by, the signal from the dotted region would not be significant, as shown in Fig. 20b. Even this small error could be reduced by improving the device accuracy. However, the dotted region will overlap with the high intensity effective area if there is a strong radiation source very close to the target point as shown in Fig. 20c. This

situation is similar to that of monitoring the temperature of the HAZ in arc welding.

According to the Stefan-Boltzmann law, the radiation intensity changes rapidly as temperature increases. Thus the effect of the overlapped area is no more negligible. It can introduce significant error into the temperature measurement near the weld pool.

Interference Measurement

Arc and weld pool interference have been reported to pose serious problems in the application of infrared detection to welding, and a great deal of effort has been made to eliminate the strong arc radiation [6]. Emissivity drifting as temperature changes is also considered one of the critical problems [7].

Several efforts were made to estimate the interference from the arc and weld pool. The first involved extinguishing the arc and simultaneously stopping the moving table. The detector output immediately after extinguishing the arc would be the net radiation from the focused area without arc interference if the signal from the weld pool is neglected[7].

Unfortunately, stopping the moving table at the same time as the arc extinguishes is not easy due to the inertia of the moving elements. Since the temperature gradient near the weld pool boundary is very high, a small position error would introduce considerable discrepancy. It is even more significant if the sensing position is ahead of the torch.

[7]Depending on the sensing position, the intensity of the pool interference is different.

The second trial was an estimation of the interference using a thermocouple. When the thermal field configuration for the case without an arc is similar to that with an arc, the signals obtained from both cases could be interpreted as the same target temperature. After getting the thermocouple and infrared radiation signals for the surface after heating by a direct welding arc and indirect heat source, the net interference effect could be estimated. The thermocouple application to actual welding for interference study has a limitation, since it is fixed on the workpiece while the arc moves. The expected interference affected signal is limited only to the time when the torch is close to the thermocouple point. It also does not measure the steady state temperature at any fixed relative distance from the arc.

The third trial was to cover the sensing point with a plate at room temperature during the steady state welding operation, for a short time. If the interference exists, the signal just after insertion does not return to an initial value but to a value of the initial signal plus the net interference. This was considered to be the most reliable method because several measurements could be made without interrupting the welding process. Fig. 21 shows one of the plotted results before analysis.

IV. CONCLUSIONS

The application of a solid state infrared array detector to weld process monitoring has been initiated. The laboratory-built sensor has been investigated and found to respond reliably, following basic radiometric theory. The investigation focused on the background or interference effects which were analysed and found to fall into 3 categories. One of them, interference by reflected radiation was found to be inevitable. The others could be minimized by using appropriate components and techniques. The total interference was found to be about 10 % of the measured steady state signal intensity near the weld pool area. This signal error is effectively less than 2 % of the temperature error due to the radiation law.

Emissivity was not found to be significantly different for the indirectly heated plates which were maintained at the same temperature, but with different surface deposits on them. However, its variation with temperature could result in a calibration error if a constant emissivity was used. Under steady-state welding conditions, the emissivity problem was not critical because the soot deposited uniformly on the weldment surface around the region of interest and the thermal field inertia was such that disturbances caused by a short period of arc instability could be neglected. It is apparent that the application of an optical filter might not be desirable to protect the arc effects when the HAZ area temperature was monitored since it reduces the signal intensity. A suitable mechanical shield showed good results.

The initial target of this research was to build a reliable camera system of the solid state infrared array detector and to demonstrate its capability as a sensor for the welding process. The final goal is to achieve an efficient and economical control using the infrared array sensor in actual welding. In spite of a number of unexpected phenomena, it is considered that the first phase of the research has provided a strong background knowledge such as the characteristics of the detector, arc spectrum, thermal response of the workpiece, the relationship between weld quality and operating parameters, and other critical information. That will be invaluable for subsequent phases of the research.

Quite a bit of effort has been made to develop a model of the dynamic response of the thermal field in the weldment, and is still in progress. This, and the results on the feedback control will be presented as the research progresses.

ACKNOWLEDGEMENT

Support of this work by the American Welding Research Council under a research grant is greatly appreciated. The infrared detector was developed and donated by the Solid State Lab in the Electrical Engineering and Computer Science Department of the University of Michigan.

References

[1] Choi, I. H., 1986, "A Silicon-Based Thermocouple Infrared Detector Array Containing On-Chip Readout Circuitry," Ph.D Thesis, Electrical Engineering and Conputer Science, The University of Michigan.

[2] Wyatt, C. L., 1978, Radiometric Calibration: Theory and Methods, Academic Press, New York, pp. 39-52.

[3] Direct Communication, Janos Technology Inc., Townshend, Vermont.

[4] Direct Communication, Molectron Detector, Inc., Campbell, Cal.

[5] The Infrared Handbook, 1978, W. L. Wolfe and G. J. Zissis eds., pp. 2-77 to 2-78.

[6] Ramsey, P. W., Chyle, J. J., et al., 1963, "Infrared Temperature Sensing Systems for Automatic Fusion Welding," *Welding Journal*, Vol. 42, pp. 338s-346s.

[7] Richardson, R. W., 1982, "Review of the State-Of-The-Art of Adaptive Control for the Gas Tungsten and Plasma Arc Welding Processes," CWR Technical Report 529501-82-5.

[8] Quigley, M. B. C., Richards, P. H., Swift-Hook, D. T., and Gick, A. E. F., 1973, "Heat Flow to the Workpiece from a TIG Welding Arc," *J. Phys. D : Appl. Phys.*, Vol. 6, pp. 2250-2258.

[9] Papoular, R., 1965, Electrical Phenomena in Gases, American Elsevier Publishing Inc., New York.

[10] Strianov, A. R. and Sventitskii, N. S., 1968, "Tables of Spectral Lines of Neutral and Ionized Atoms," IFI/Plenum, New York.

[11] Luken, W. E. and Morris, R. A., 1982, "Infrared Temperature Sensing of Cooling Rate for Arc Welding Control," *Welding Journal*, Vol. 61, pp. 27-33.

[12] Boillot, J. P., Cielo, P., et al., 1985, "Adaptive Welding by Fiber Optic Thermographic Sensing : Analysis of Thermal and Instrumental Conditions," *Welding Journal*, Vol. 64, pp. 209s-217s.

[13] Glickstein, S. S., 1986, "Temperature Measurements in a Free Burning Arc," *Welding Journal*, Vol. 65, pp. 222s-229s.

[14] Lancaster, J. F., 1984, The Physics of Welding, Pergamon Press Inc., New York.

[15] Cambell, A. B., 1963, "Plasma Physics and Magnetofluid Mechanics," McGraw-Hill Book Co. Inc., New York.

[16] Ton, H., 1975, "Physical Property of the Plasma-MIG Welding Arc," *J. Phys. D: Appl. Phys.*, Vol. 8, pp. 922-933.

[17] Howden, D. G., 1969, "Mass Transfer of Metal Vapor and Anode Temperatures in Arc Melting," *Welding Journal*, Vol. 48, pp. 125s-132s.

[18] Tidwell, E. D., 1972, "Transition Probabilities of Argon II," *J. Quart. Spectrosc. Radiat.*, Vol. 12, pp. 431-441.

[19] Key, J. F., Chan, J. W., and McIlwain, M. E., 1983, "Process Variable Influence in Arc Temperature Distribution," *Welding Journal*, Vol. 62, pp. 179s-184s.

[20] Essers, W. G. and Walter, R., 1981, "Heat Transfer and Penetration Mechanisms with GMA and Plasma-GMA Welding," *Welding Journal*, Vol. 60, pp. 37s-42s.

Appendix: Spectrum of the Radiation from a Welding Arc

Quantum physics explains the optical spectra of a gas when it absorbs external energy and emits radiation. As a gaseous conductor, the welding arc converts electrical energy into heat, and the internal and kinetic energies of the particles in the arc are changed through inelastic collisions with other particles. If the energy exchanged is high enough, some of the electrons of the gas atoms are excited; the internal energy of the atom is then increased by the amount $\Delta U = eV^*$ which is the difference between the energies of the initial and final states of the electrons. The initial state of the particle does not necessarily correspond to the ground state.

The reaction of one of the typical excitation mechanisms is represented as [9]

$$h\nu + A \longrightarrow A^* \qquad (A1)$$

where A and A^* are neutral atoms or molecules in the inital and excited states respectively, ν frequency of the photon, h Planck's constant ($= 6.6 \text{ x } 10^{-27} ergsec$).The reaction threshold is defined as

$$h\nu = eV^* \qquad (A2)$$

with eV^* as change of the internal energy for an excited atom. From $\lambda\nu = c$ (speed of light: $3 \text{ x } 10^{10} cm/sec$), the wavelength of radiation is

$$\lambda = \frac{12400}{V^*}(\mathring{A}) \qquad (A3)$$

where V^* is the change of the internal energy in electron-volts.

The excitation is the change of the energy level of an electron within an atomic boundary. Naturally, its energy is less than the ionization energy, which will be explained below. The change of energy level or the transition from one quantized state to another is governed by a specific rule or selection rule. Thus, an electron could transit back and forth between any two energy levels which satisfy this rule if there is adequate external energy. However, the probabilities are much different, depending on the transitions. This difference results in the varieties of spectral intensities.

In spite of enormous theoretical research in plasma spectroscopy, the experimental observations of spectral lines for various elements are more convenient for evaluating the spectral characteristics of the welding arc. Many published tables and research work list the spectral lines of neutral and ionized atoms. For the argon arc, the range of the wavelength found in these data is from 395.92 $\mathring{A}$ (E_h=0, E_b=31.31 eV) to 25660.9 $\mathring{A}$ (E_h=14.25 eV, E_b=14.74 eV) over the neutral, singly and doubly ionized atoms [10]. However, the spectral intensities are relatively weak around the observed maximum wavelength region. Also, a school of thought argues that a longwave pass optical filter with 2 μm cutoff frequency is enough to prevent the arc interference effects on the detector [11, 12]. A typical spectroscopy [13] in the ultraviolet region of the argon arc is shown in Fig. 22.

From atomic structure, it is clear that the ionization potential, $V_i > V^*$. The ionization mechanism is

$$h\nu + A \longrightarrow A^+ + e^- \qquad (A4)$$

Eq. (A4) is possible only when

$$h\nu \geq eV_i \tag{A5}$$

and the wavelength of the resulting radiation is

$$\lambda \leq \frac{12400}{V_i}(\mathring{A}) \tag{A6}$$

with V_i in electron-volts.

Only a portion of the atoms in an arc is ionized depending on the gaseous material, temperature and pressure. The degree of single ionization, α_i, can be expressed as a Saha Equation [14] :

$$\frac{\alpha_i}{1-{\alpha_i}^2}p = (\frac{2\pi m_e}{h^2})^{\frac{3}{2}}(\kappa T)^{\frac{5}{2}}\frac{2z_+}{z}\exp(-\frac{eV_i}{\kappa T}) \tag{A7}$$

where p is the pressure in atmosphere unit, m_e mass of electron, h Planck's constant, κ Boltzmann's constant, z_+ partition function of ion, z partition function of neutral atom, V_i first ionization voltage. For argon atom [15],

$$Z(T) = 1 + 60e^{-\frac{162500}{T}} + ... \tag{A8}$$

$$Z_+(T) = 4 + 2e^{-\frac{2062}{T}} + 2e^{-\frac{156560}{T}} + ... \tag{A9}$$

Thus, $Z(T)$ is approximated as 1 and $Z_+(T)$ as the first 2 terms for the arc temperature range.

Spectral measurement indicates that there exists metal vapor in the arc core of a plasma-MIG welding where the electrode melts and the molten drops are detatched downward [16]. Vapor from the workpiece is also reported in the GTAW process [17]. Thus, the same phenomenon is expected for the conventional GMA welding too. From the Saha equation, it is clear that metal atoms are more

Table 5: Ionization Potentials for Various Elements[10]

Element	V_{i1} (eV)	V_{i2} (eV)	V_{i3} (eV)
Fe	7.897	16.187	30.647
Cu	7.726	20.291	36.834
Si	8.151	16.345	33.491
Ar	15.759	27.628	40.908
C	11.269	24.381	47.881
He	24.586	54.414	
N	14.548	29.611	47.436
O	13.617	35.146	54.935

highly ionized and excited than argon due to the relatively low ionization voltages as shown in Table 5.

Considering the radiation effect from arc to detector, the spectral intensity is as important as the spectral range of arc elements. Actual radiation intensity is the summation of the individual spectral intensities all over the spectral lines. Under the assumption of local thermodynamic equilibrium in the arc, the spectral intensity I_λ of any element at temperature T can be estimated [16, 18, 19], as

$$I_\lambda = gA_\lambda \frac{hc}{\lambda} \frac{n(T)}{Z(T)} e^{-\frac{E}{\kappa T}} \qquad (A10)$$

where g is the statistical weight of the initial state, A_λ the transition probability of the atomic line (s^{-1}), $n(T)$ the atomic density, $Z(T)$ the partition function for

Table 6: Composition of Plasma-Mig Welding Arc [16]

		Atomic Density ($x10^{-15}$)	Ion and Electron Density ($x10^{-15}$)
Inner Arc	Fe	10.0	8.0
	Mn	2.5	2.8
	Cu	1.5	0.4
	Ca	0.01	0.2
	Ar	1042	0.005
Outer arc	Ar	265	143

neutral atoms, T the temperature (K), E the energy of the initial state, and κ Boltzmann constant(=1.38 x 10^{-23} J/K).

Each element has the same order of average atomic conditions such as transition probability, statistical weight, or energy levels. However, the difference of atomic densities between metal vapor and argon is significant as shown in Table 6. This can be supported from the thermodynamical relationship between vapor pressure and temperature. In steady state, Fe vapor is in equilibrium with other particles in the welding arc. Then, the partial pressure of any element is proportional to the ratio of the number of the neutral or ionized atoms to the total gas particles.

There are wide range of varieties in the measured drop and weld pool tem-

peratures depending on the researchers' welding conditions and experimental methods. In GMAW for steel, the range of weld pool temperature is from 1900° to 2100° C. For the drop temperature, it is from 2000° to 2700° C [14]. But the molten drop temperature is always much higher than that of the weld pool, and its superheated thermal content assists to melt the workpiece [20]. However, the vapor pressure is very sensitive to the temperature as shown in Fig. 23. Thus the metal vapor from the weld pool will be negligible compared to that from the molten metal drops of the electrode wire.

From Fig. 23, Fe vapor pressures corresponding to the drop temperatures are about 1 to 100 mmHg. This means that the percentage of Fe atoms is 0.13 to 13 % of all the arc particles in the core region of the arc where metal vapor exists. If the drop temperature is around 2300° C, the percentage of Fe is 1.5 %. It is the same range as the data in Table 6. However, the metal vapor rich zone is a relatively small region compared to the whole volume of arc. Thus, it can be concluded that the radiation from metal vapor has negligible effect on the detector response compared to that from argon.

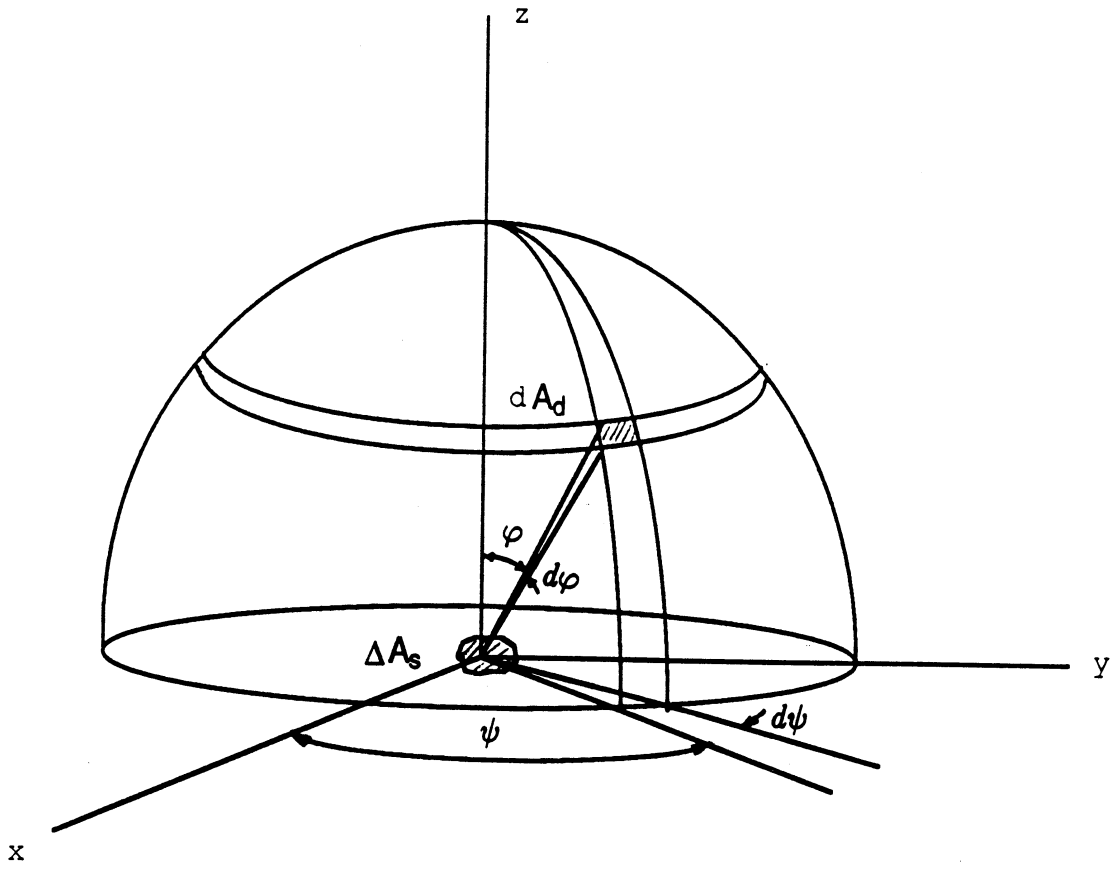

Fig. 1 Radiation from surface element to surrounding [2]

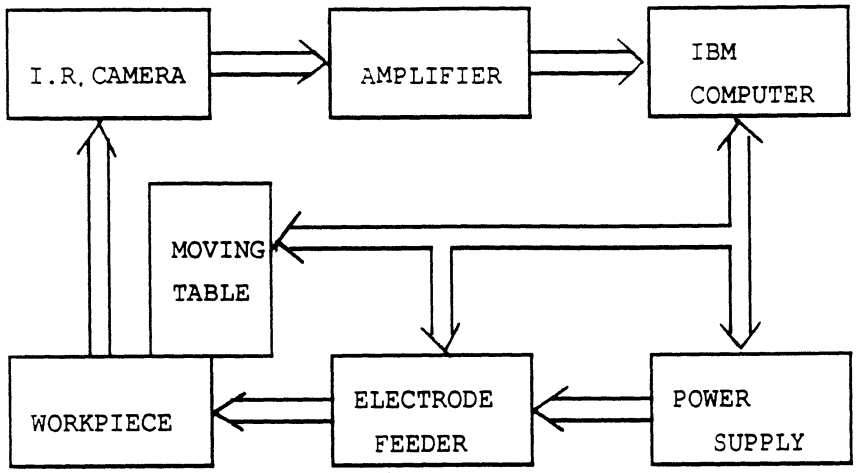

(a)

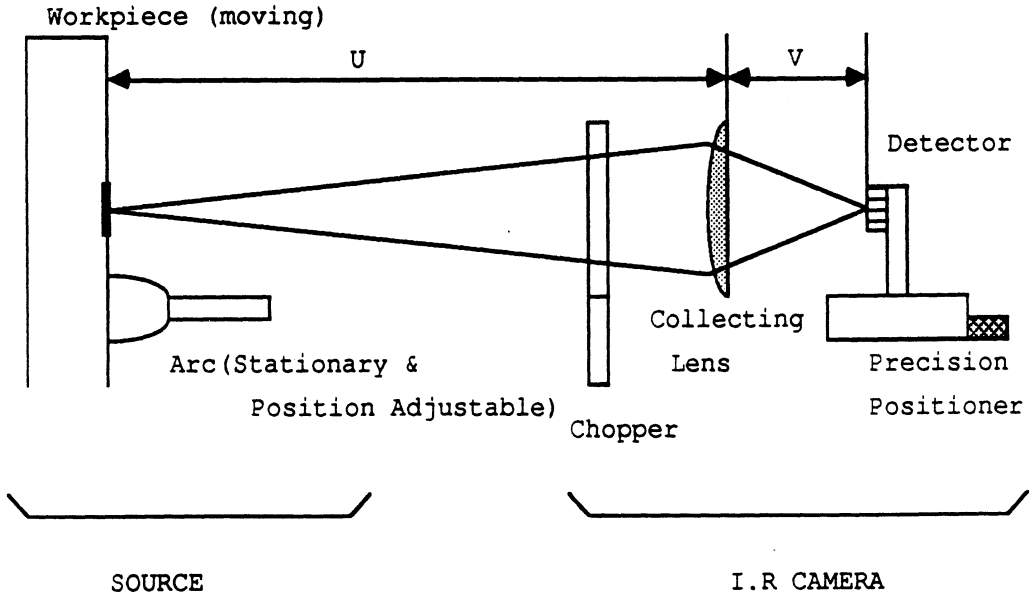

(b)

Fig. 2 Infrared detecting system: (a) welding and infrared detecting system, (b) schematic diagram of infrared system.

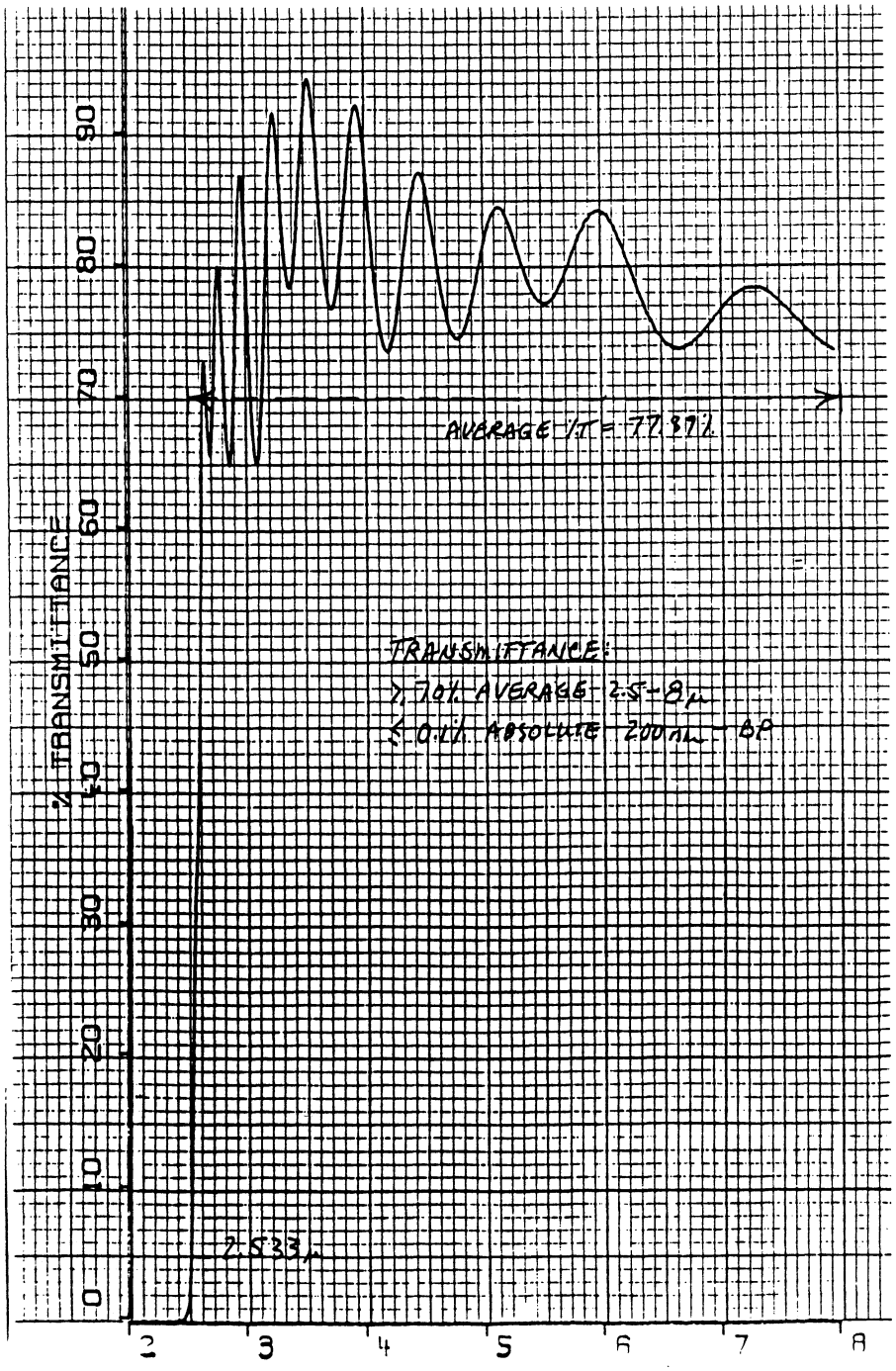

Fig. 3a Calibration chart for optical filter 1: Germanium [12]

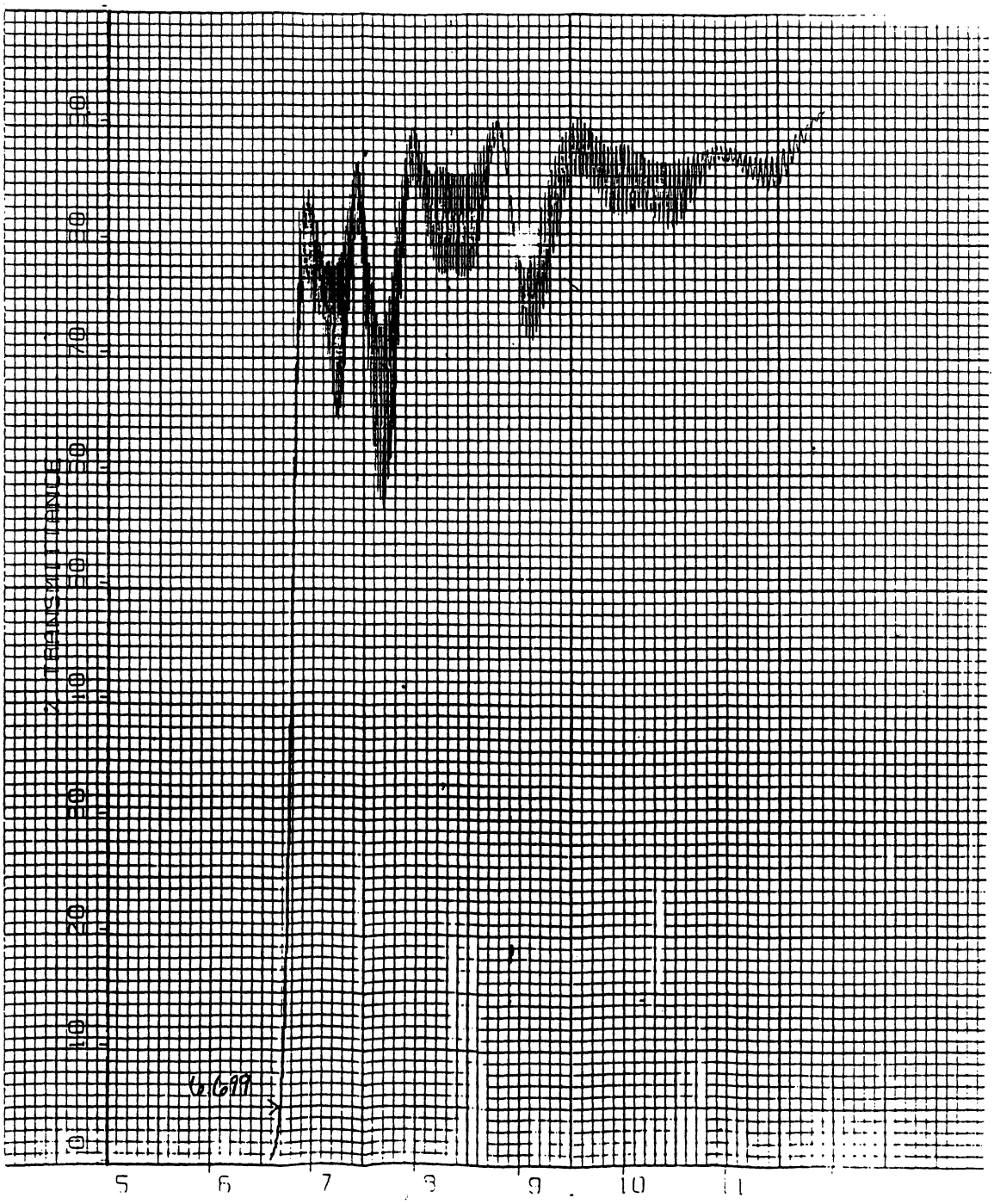

Fig. 3b Calibration chart for optical filter 2: Silicon [12]

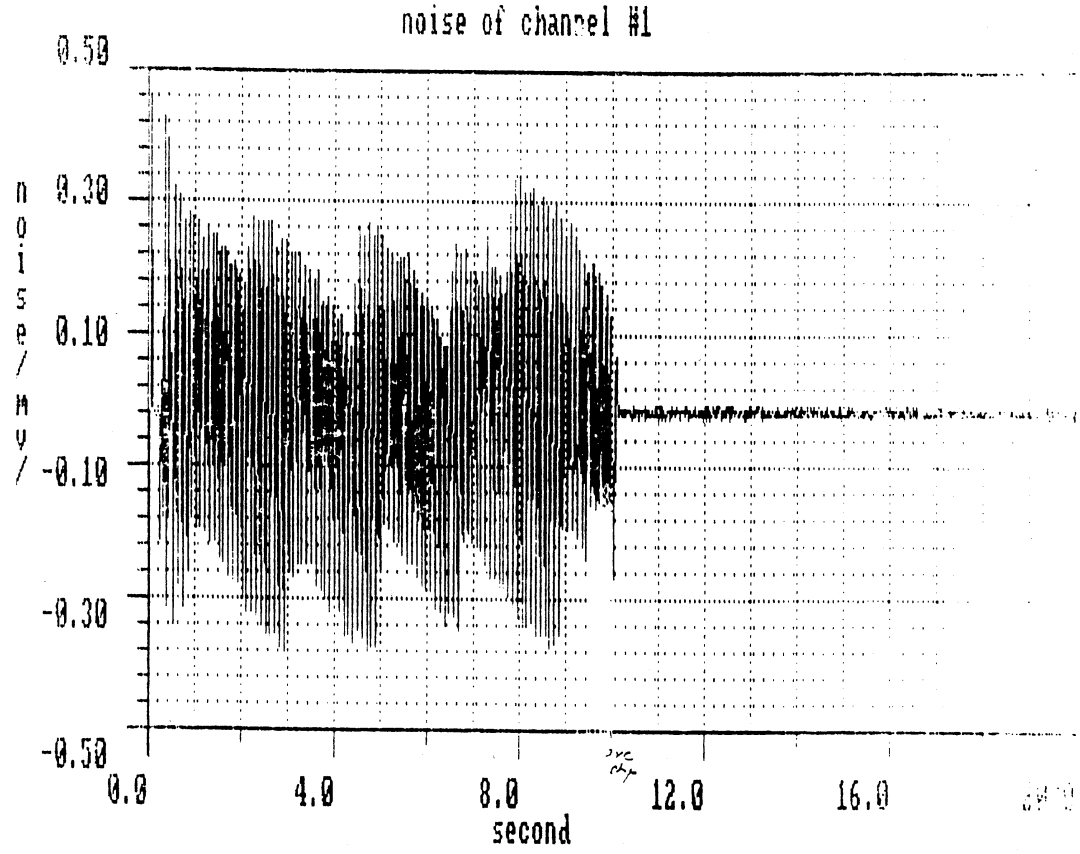

(a)

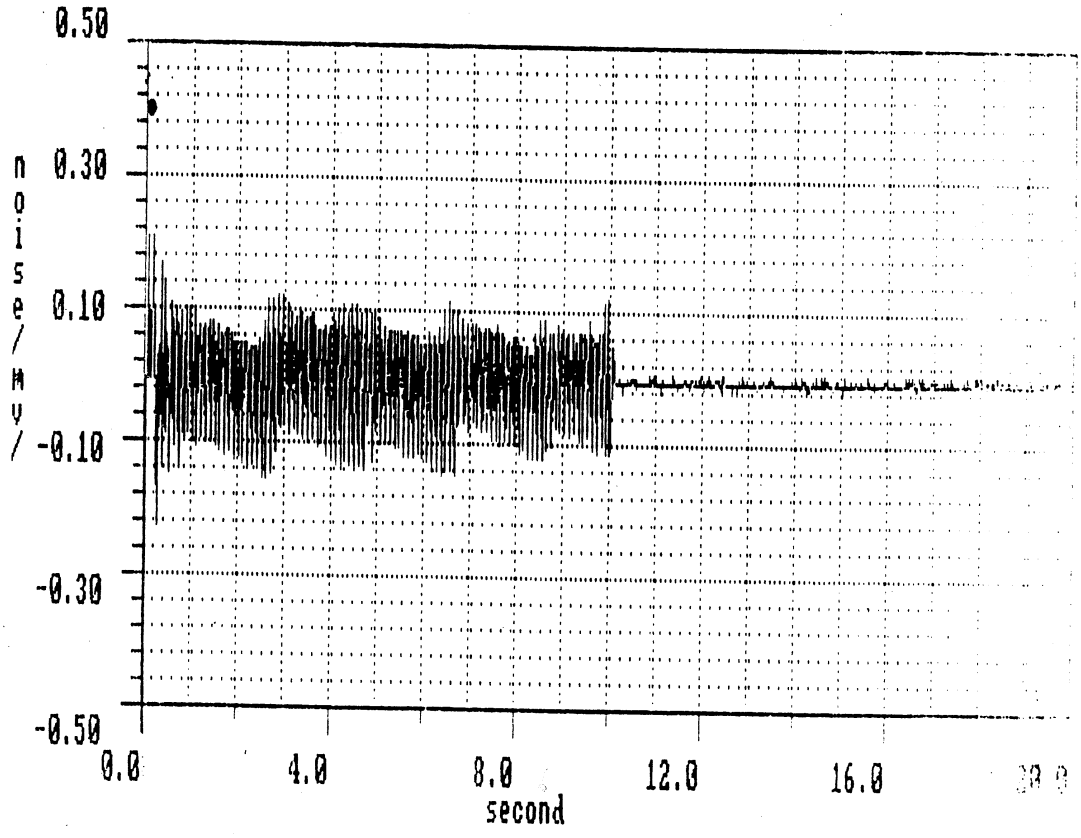

(b)

Fig. 4 Detector noise with optical filter 2. (a) channel #1, (b) channel #3.

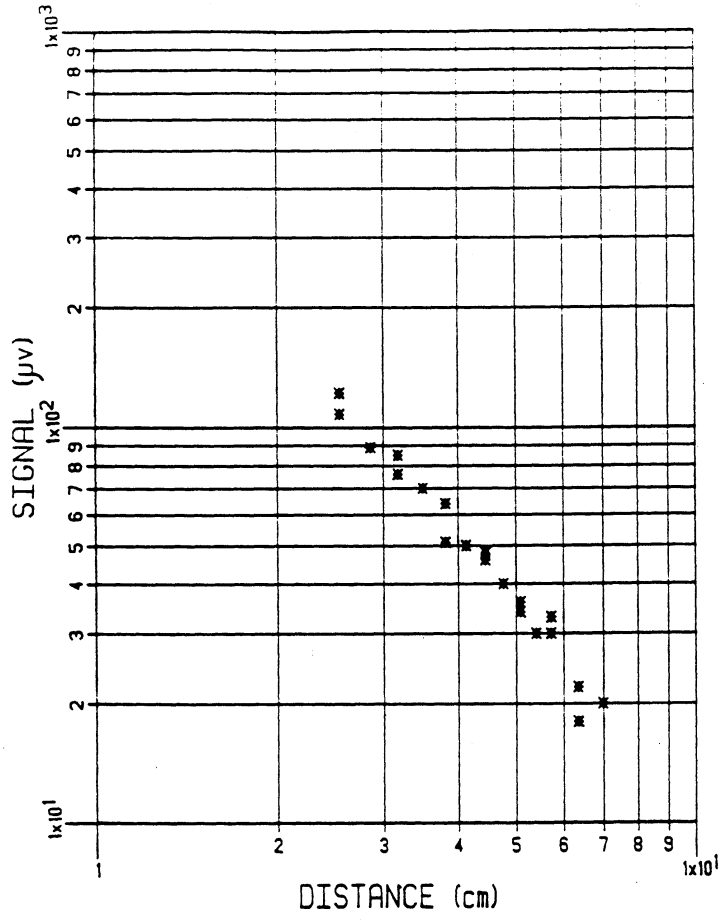

(a)

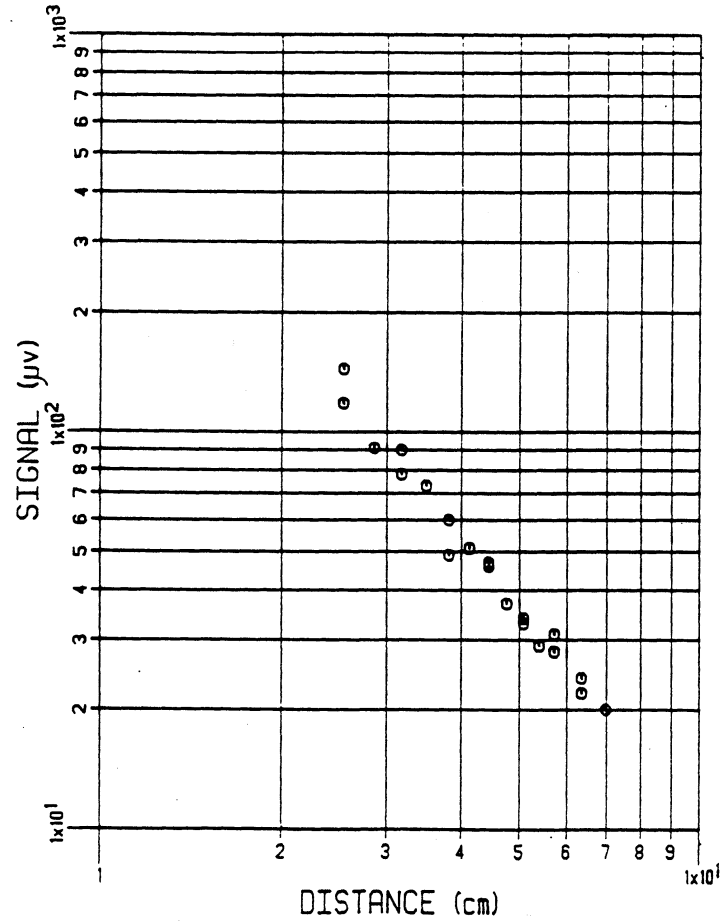

(b)

Fig. 5 Response of infrared detector without collecting lens.
Target is a 500° K blackbody.: (a) channel #1, (b) channel #2.

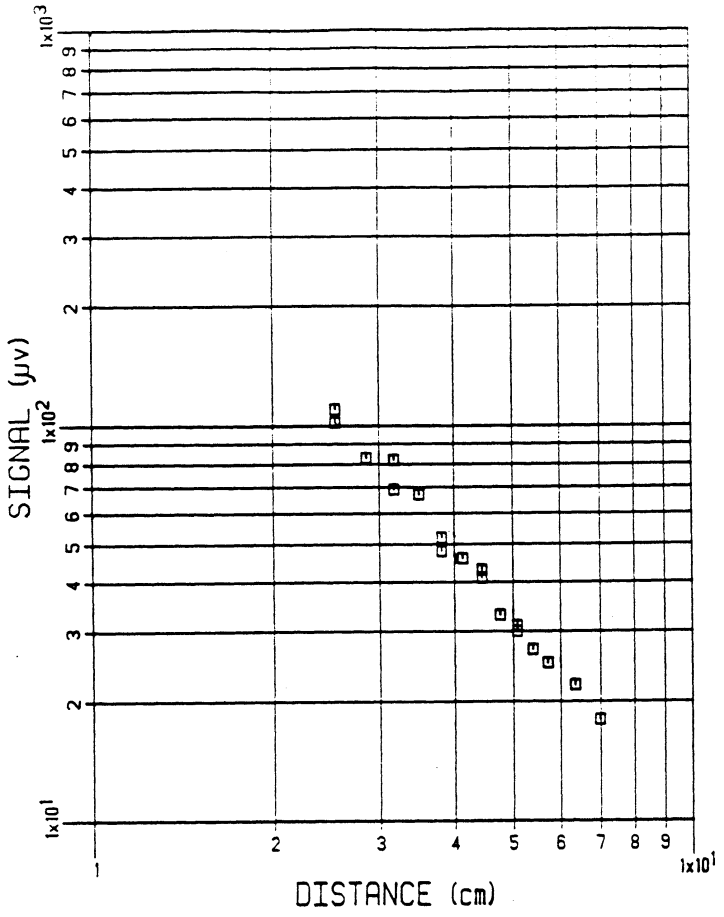

(a)

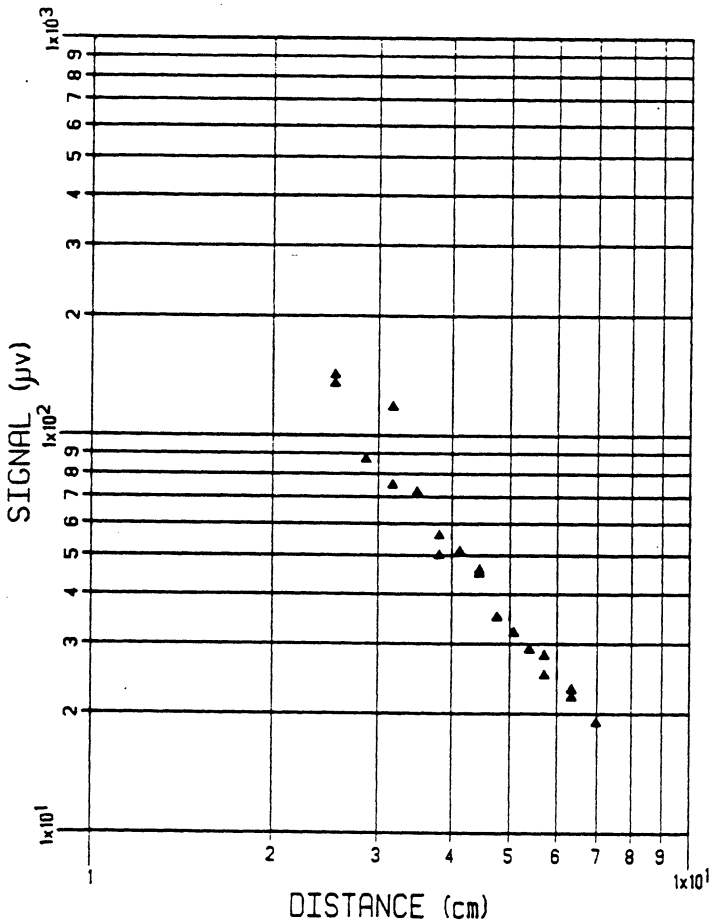

(b)

Fig. 6 **Response of infrared detector without collecting lens. Target is a 500° K blackbody.: (a) channel #3, (b) channel #4.**

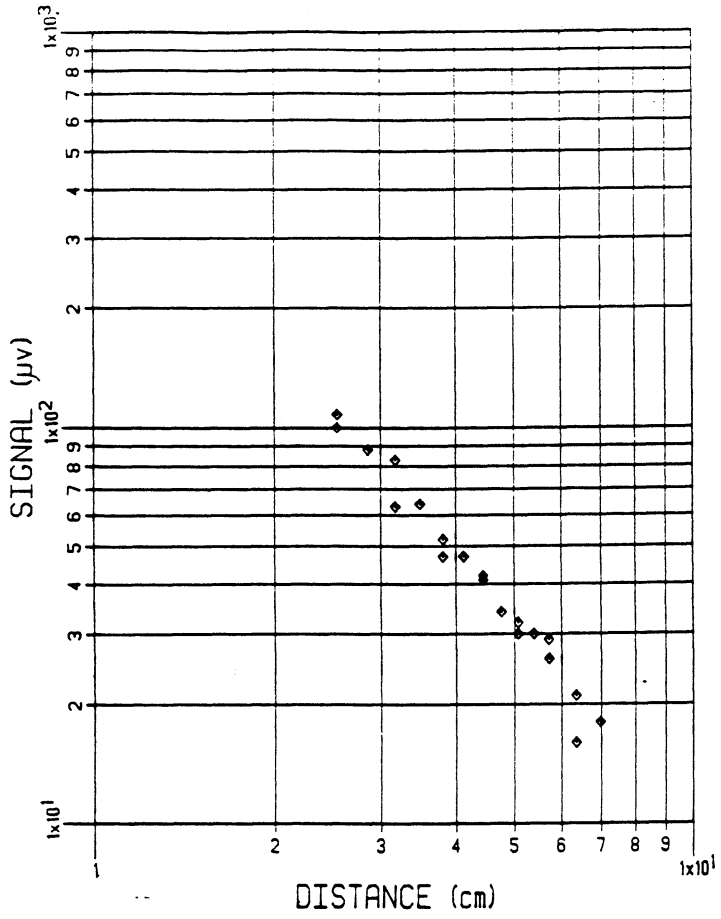

(a)

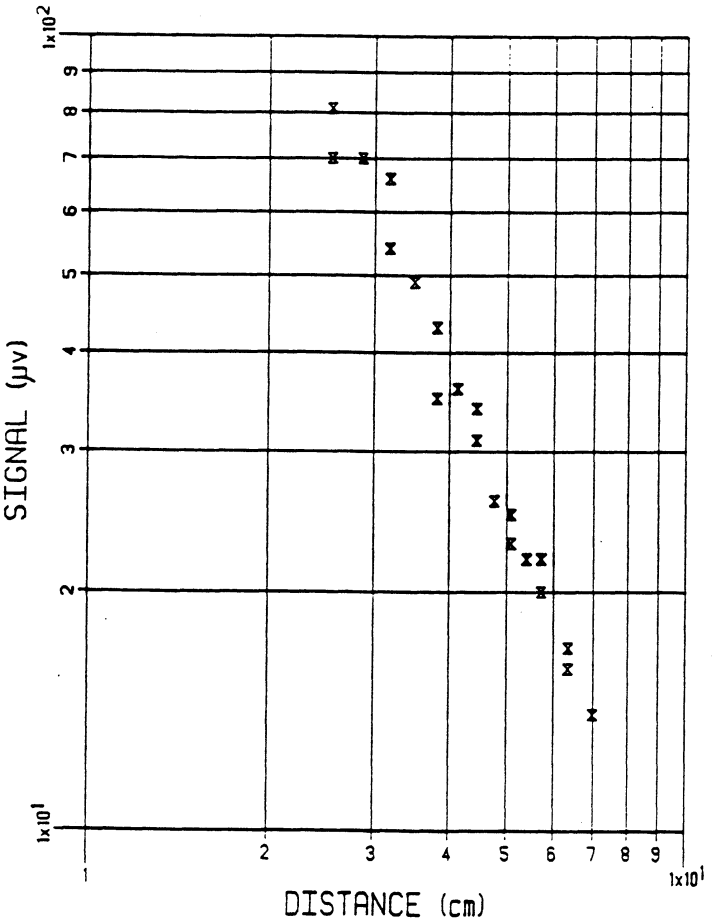

(b)

Fig. 7 **Response of infrared detector without collecting lens. Target is a 500° K blackbody.: (a) channel #5, (b) channel #6.**

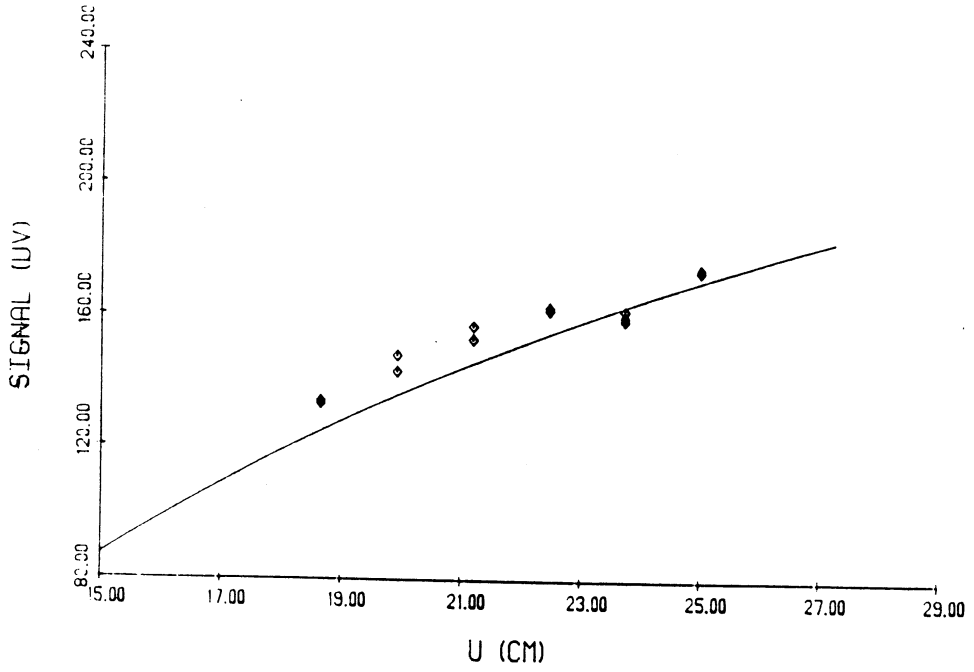

(a)

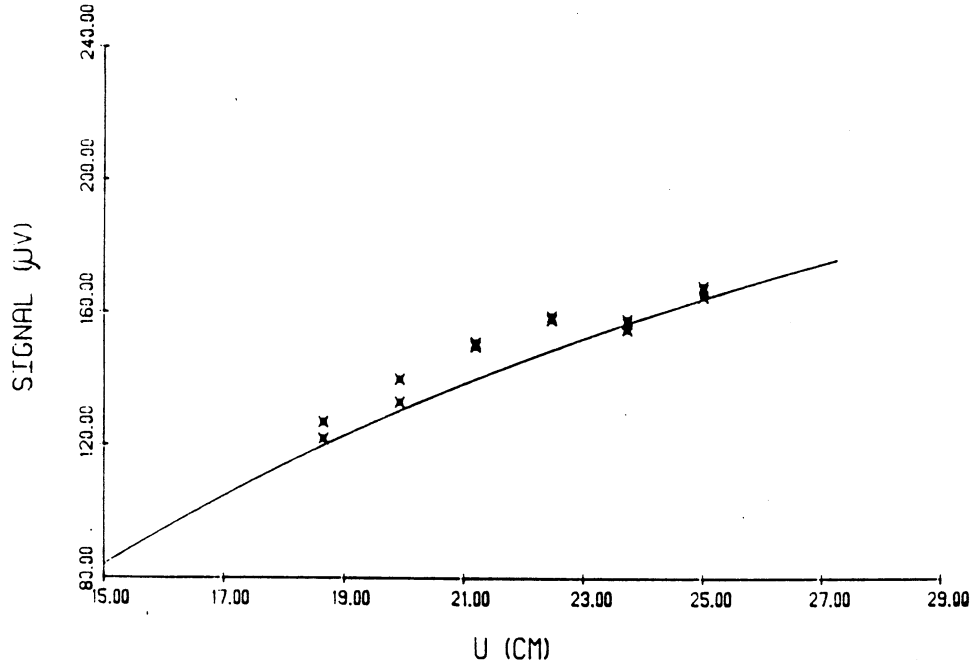

(b)

Fig. 8 Response of infrared detector with collecting lens.
Target is a 500° K blackbody.: (a) channel #1, (b) channel #2.
mark: experiments, solidline: theoretical curve.

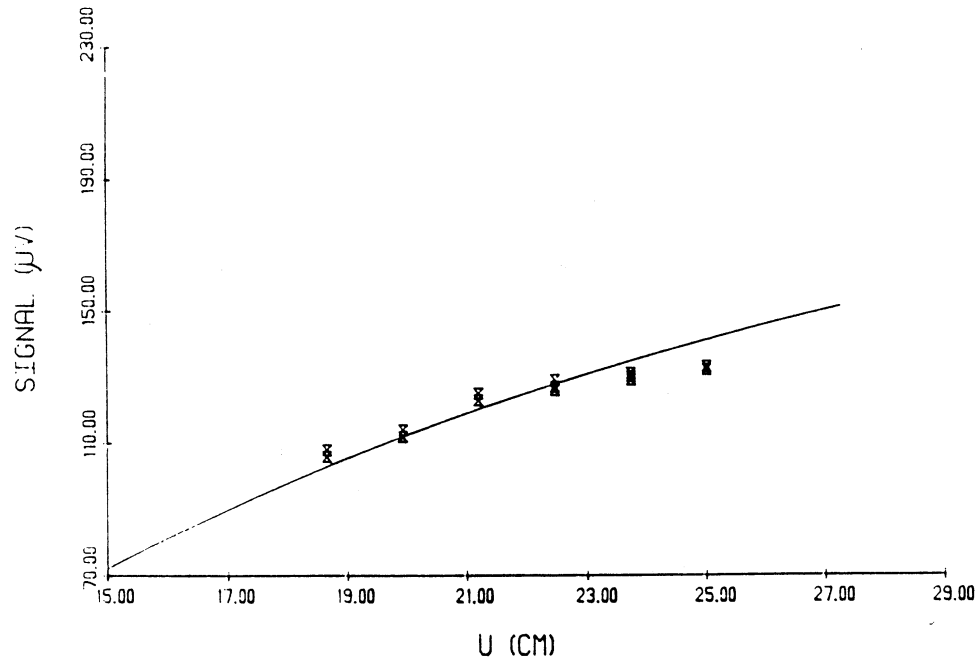

(a)

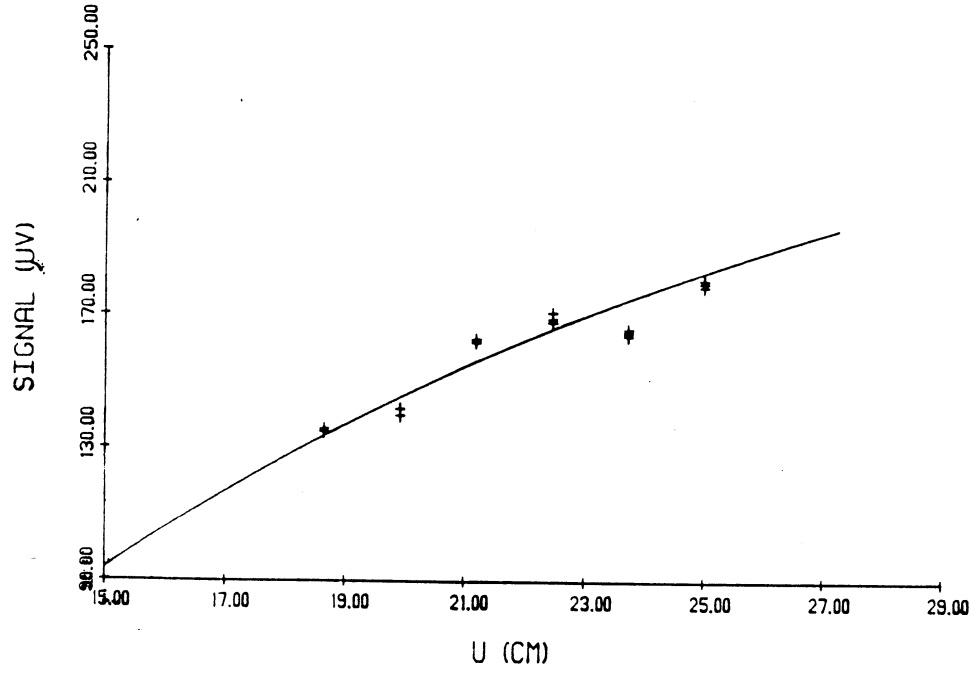

(b)

Fig. 9 Response of infrared detector with collecting lens.
Target is a 500° K blackbody.: (a) channel #3, (b) channel #4.
mark: experiments, solidline: theoretical curve.

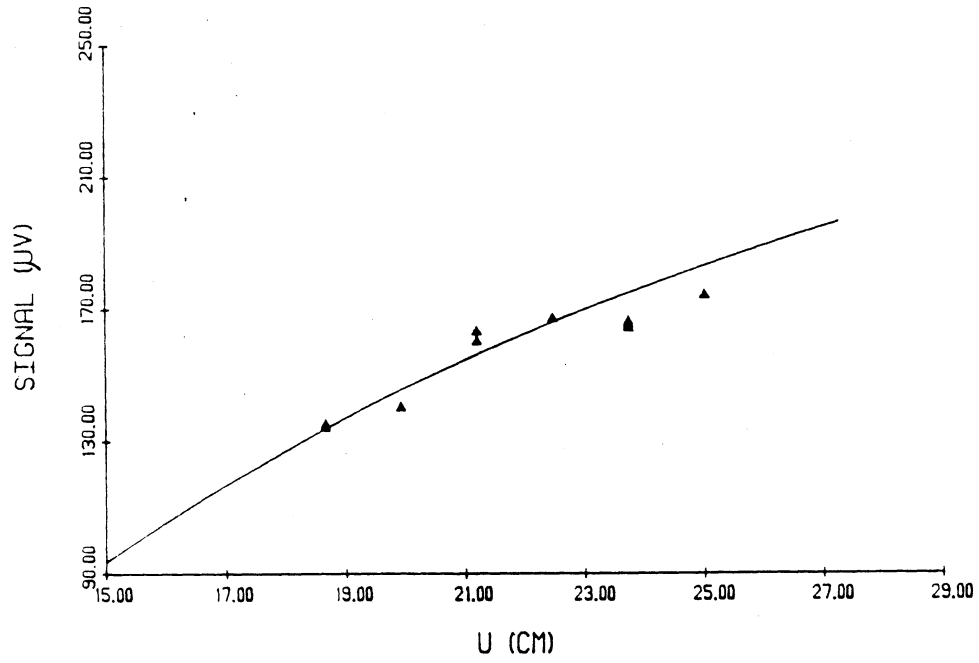

(a)

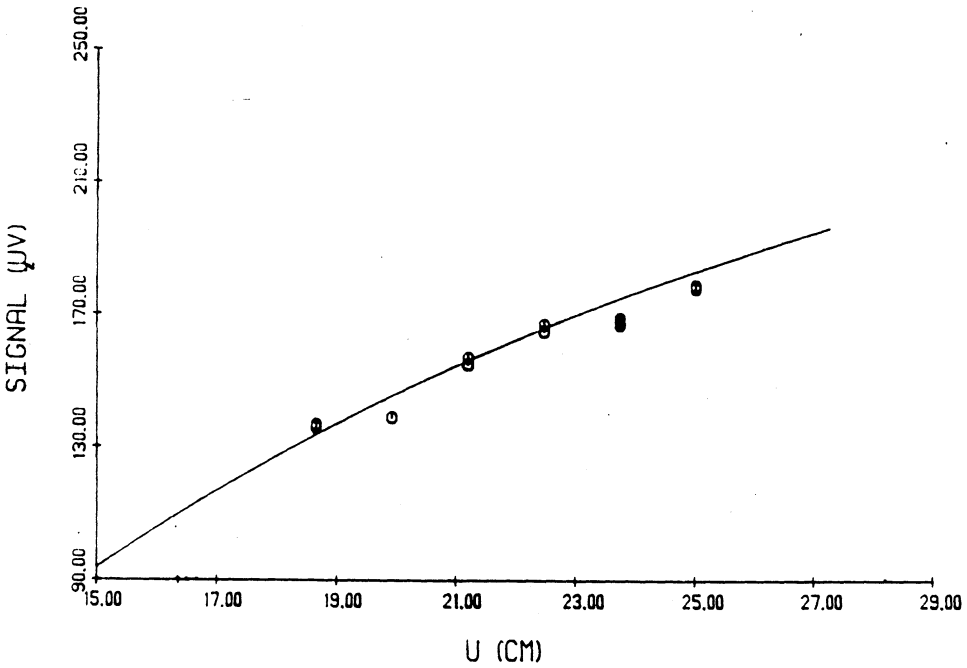

(b)

Fig. 10 **Response of infrared detector with collecting lens. Target is a 500° K blackbody.: (a) channel #5, (b) channel #6. mark: experiments, solidline: theoretical curve.**

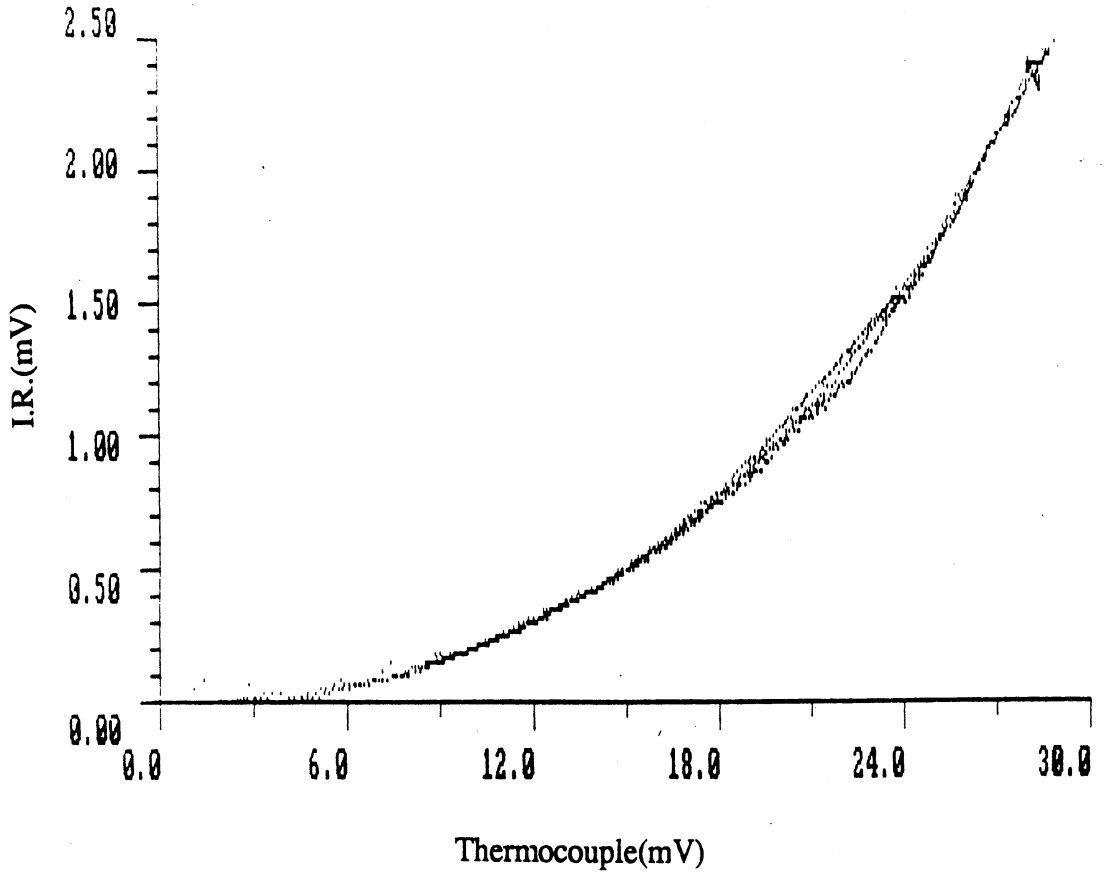

Fig. 11 Comparision of infrared detector and thermocouple output.
K-type thermocouple is at target point. 2 heating and 1 cooling curves.

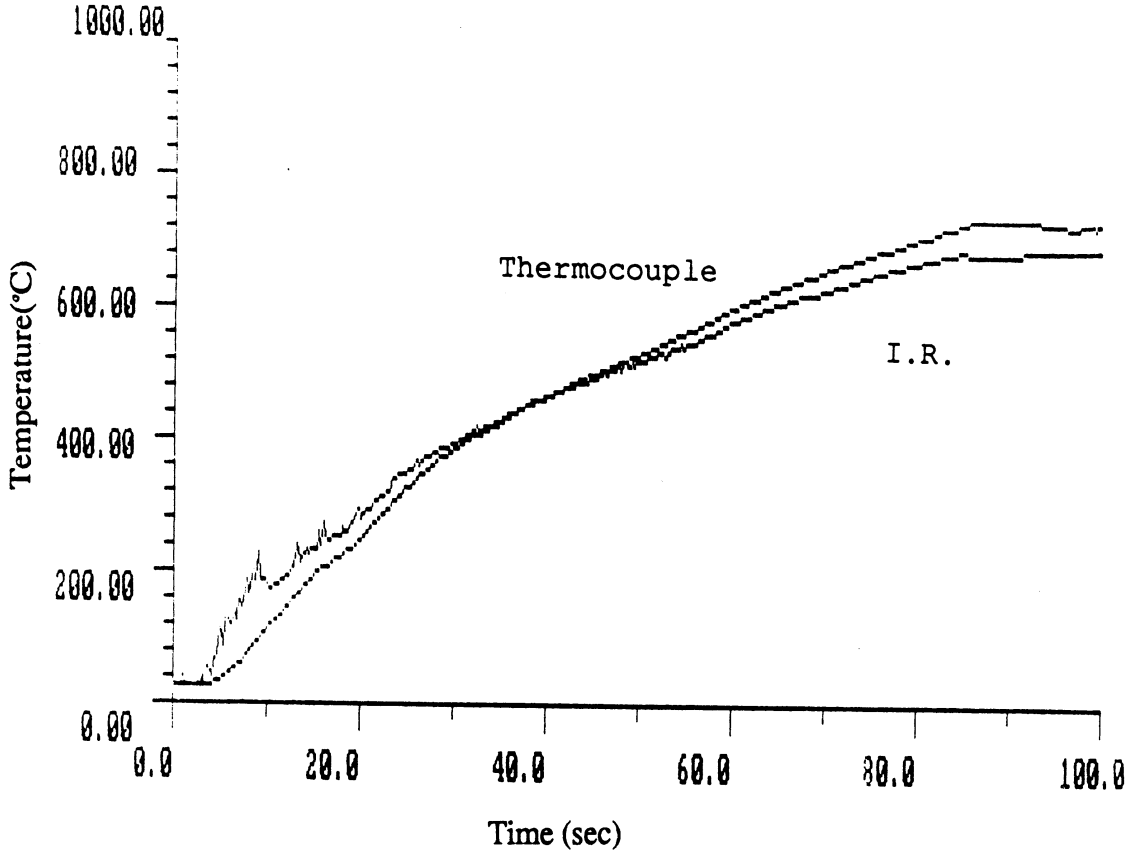

Fig. 12 A typical plot of infrared and thermocouple responses
Which are calibrated to temperature. Initially, unsmooth curve is for the infrared detector, and smooth one is for the K-type thermocouple.

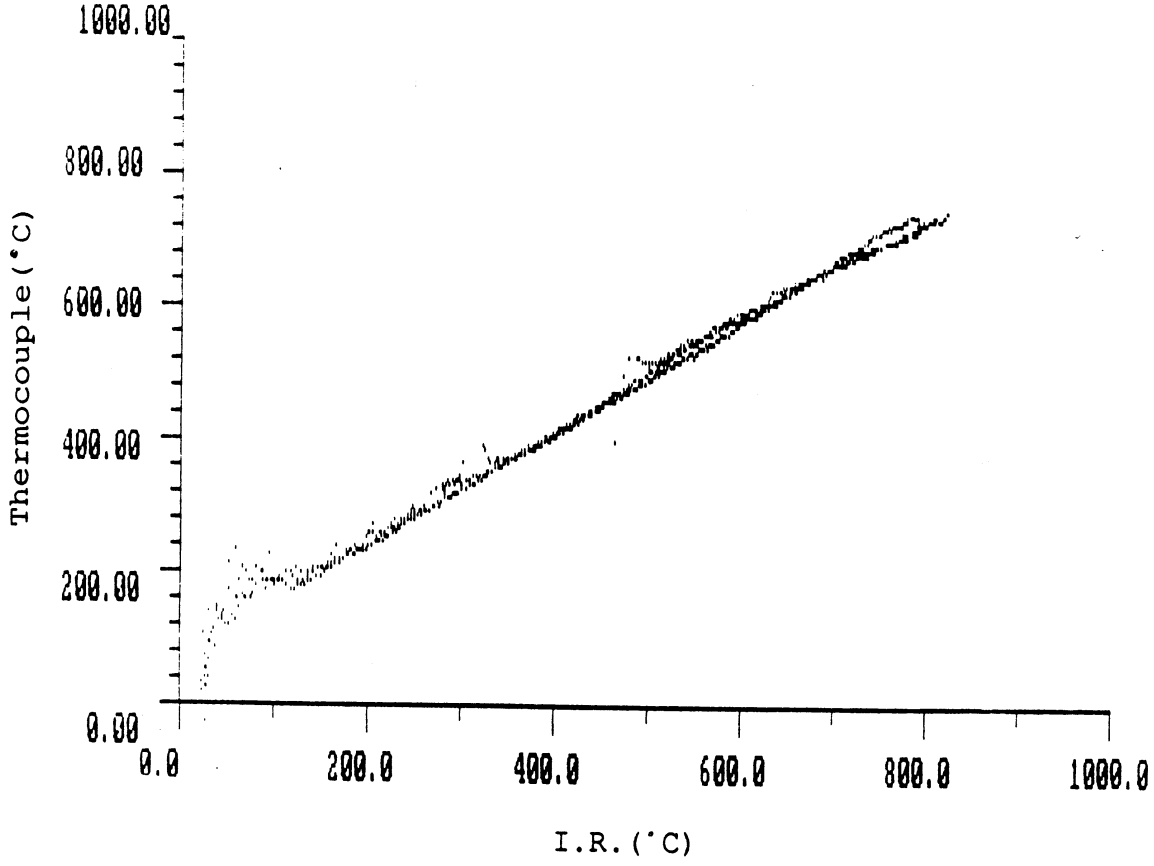

Fig. 13 Plots of temperature calibrated infrared signals vs. thermocouple measured values.

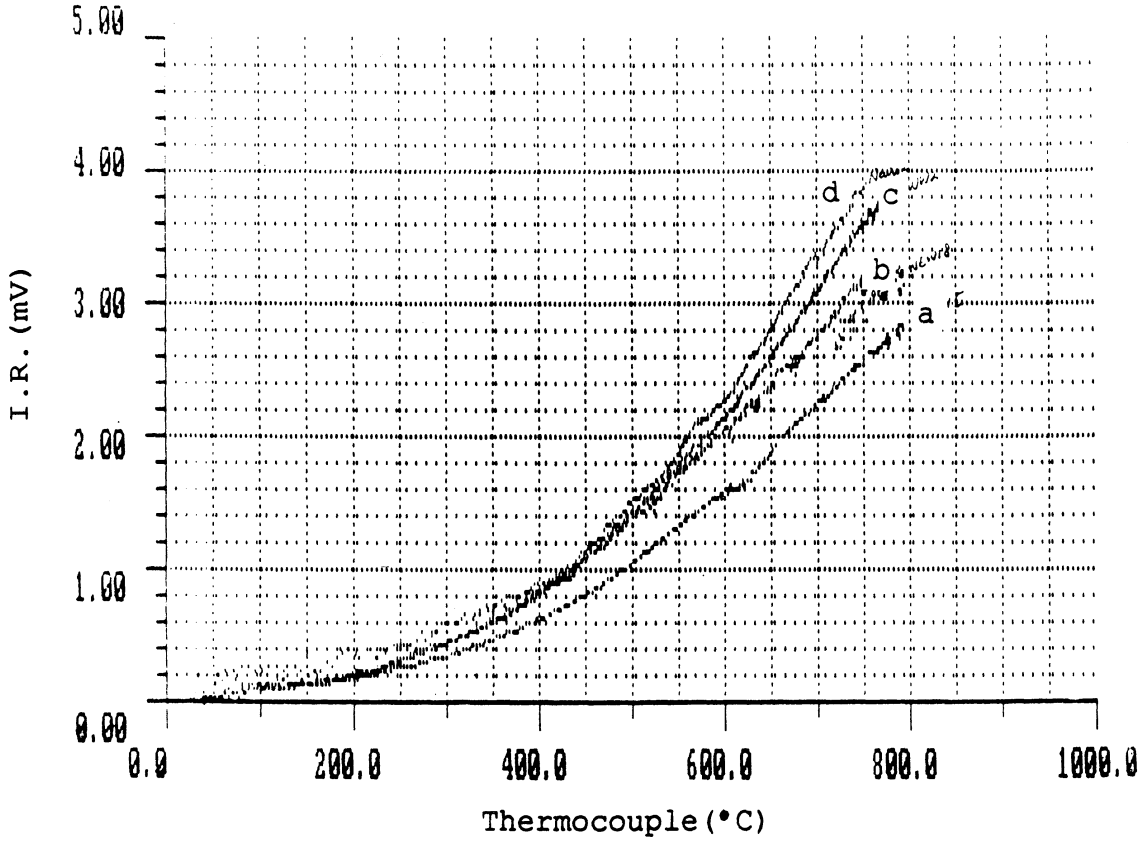

Fig. 14 Plots showing emissivity effect on infrared detector signals (a)clean, (b)oxide, (c)candle soot and (d)welding soot.

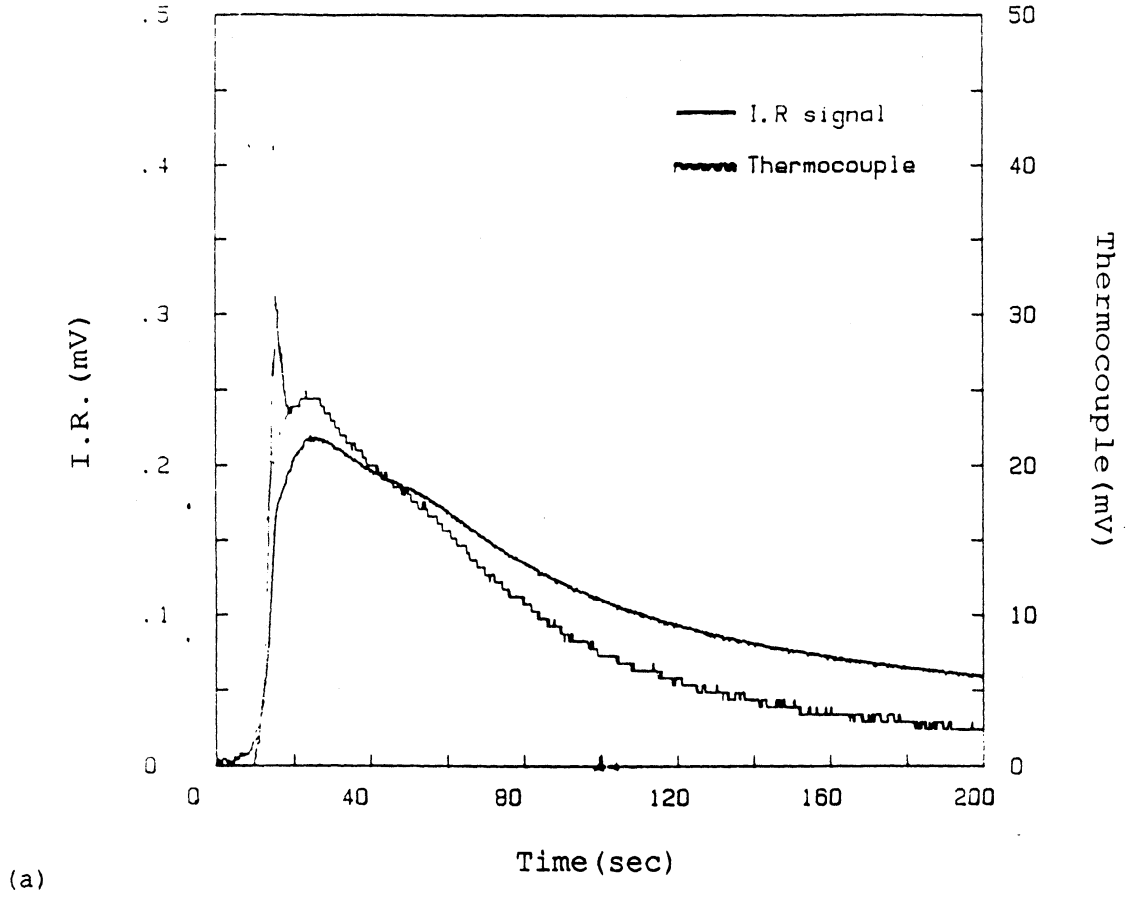

(a)

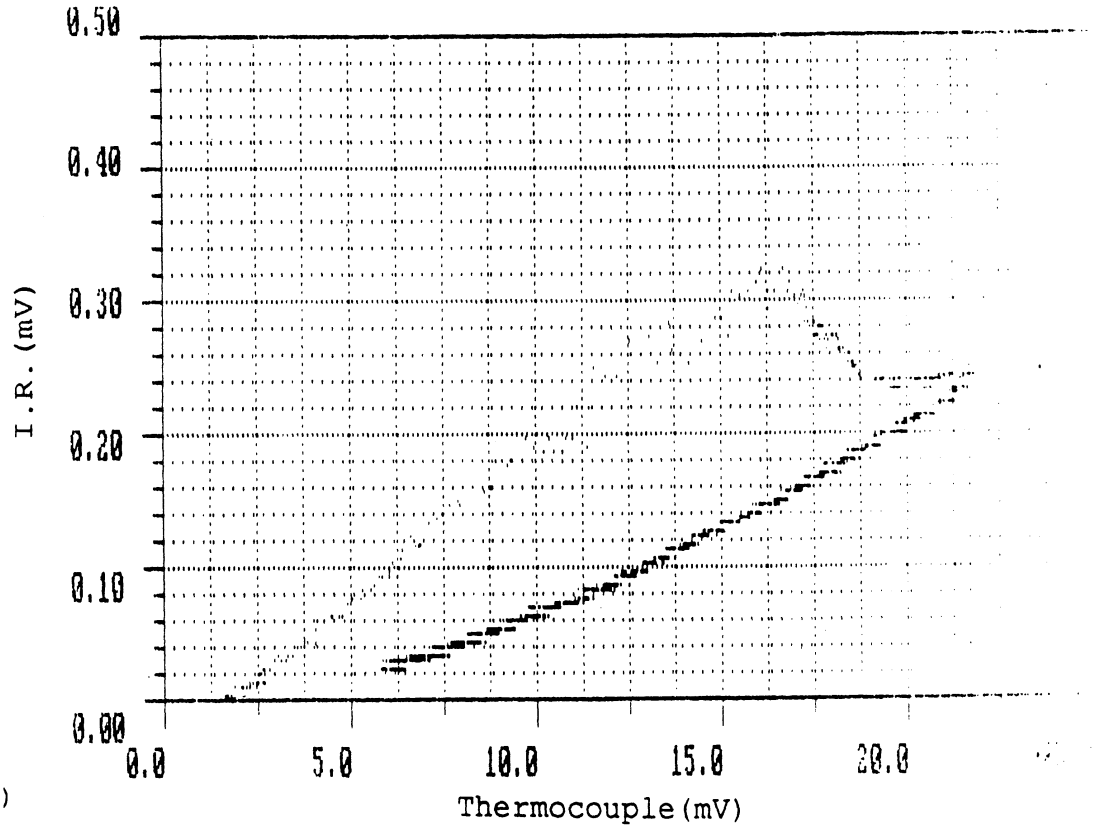

(b)

Fig. 15 Infrared and thermocouple signals during welding with optical filter 2 (1.0 inch diameter, transmitts 7 ~ 12 μm wavelength)

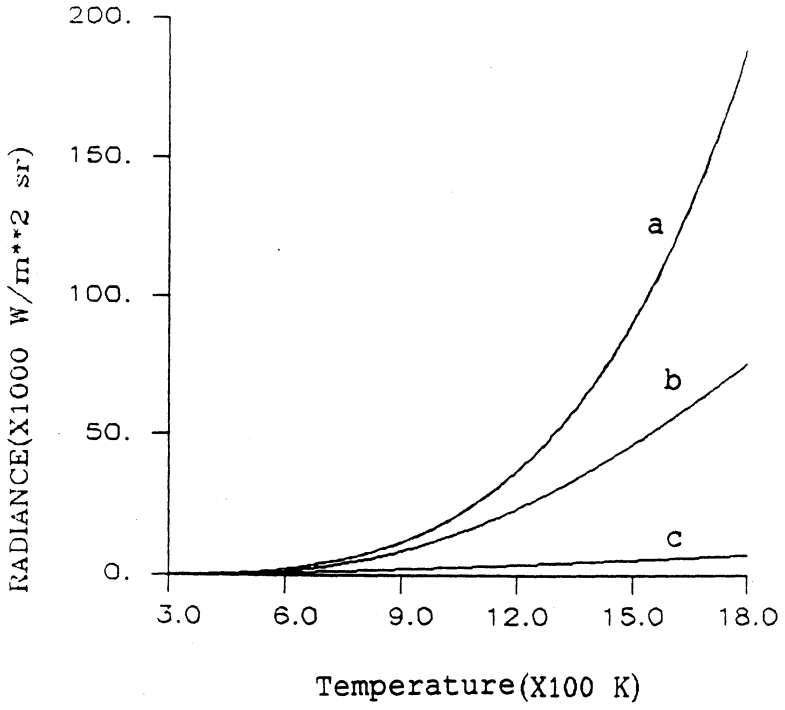

Fig. 16 Radiant intensity through optical elements. (a) without optical element and ZnSe lens (b) filter1, (c) filter 2.

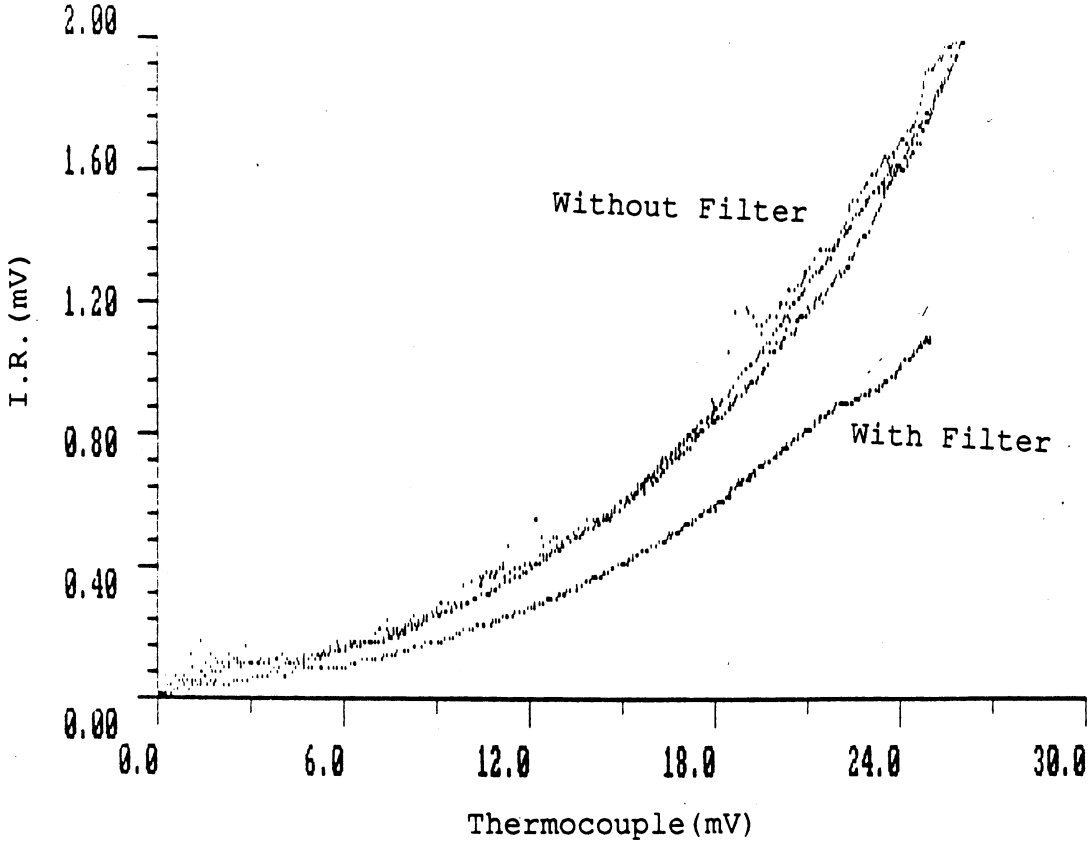

Fig. 17 3 measurement plots of infrared detector without optical filter and 1 with optical filter (1.0 inch diameter, located after lens, transmitts 2.5 $\sim$ 8 μm).

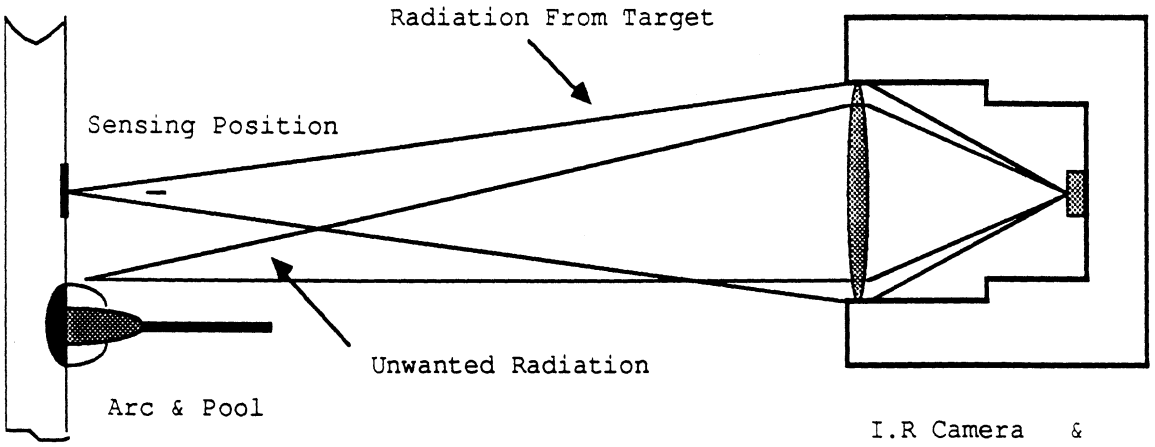

(a)

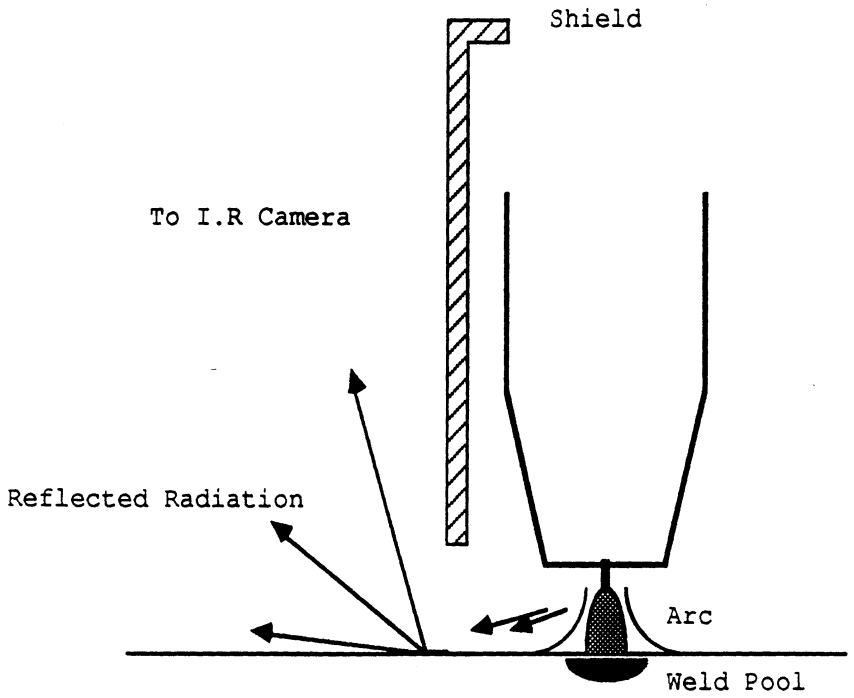

(b)

Fig. 18 Interference mechanisms: (a) stray radiation, (b) reflected radiation.

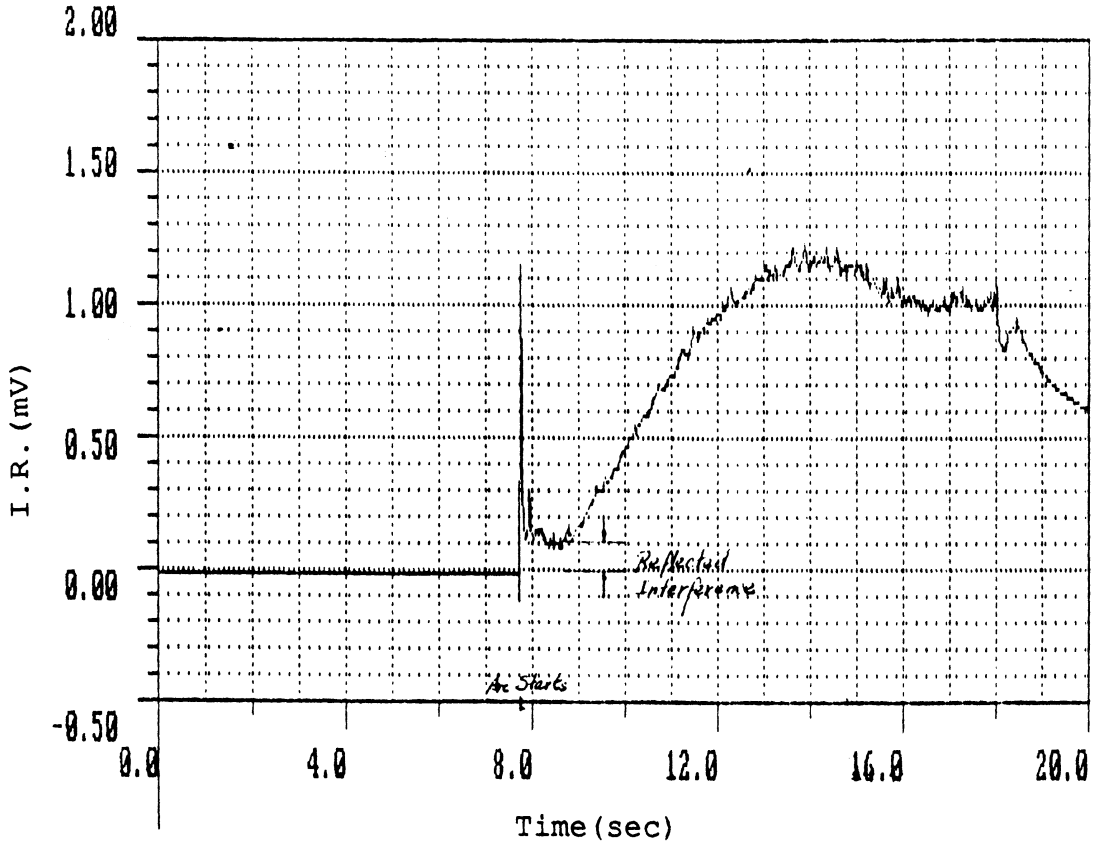

Fig. 19 Reflected radiation in the signal plot.

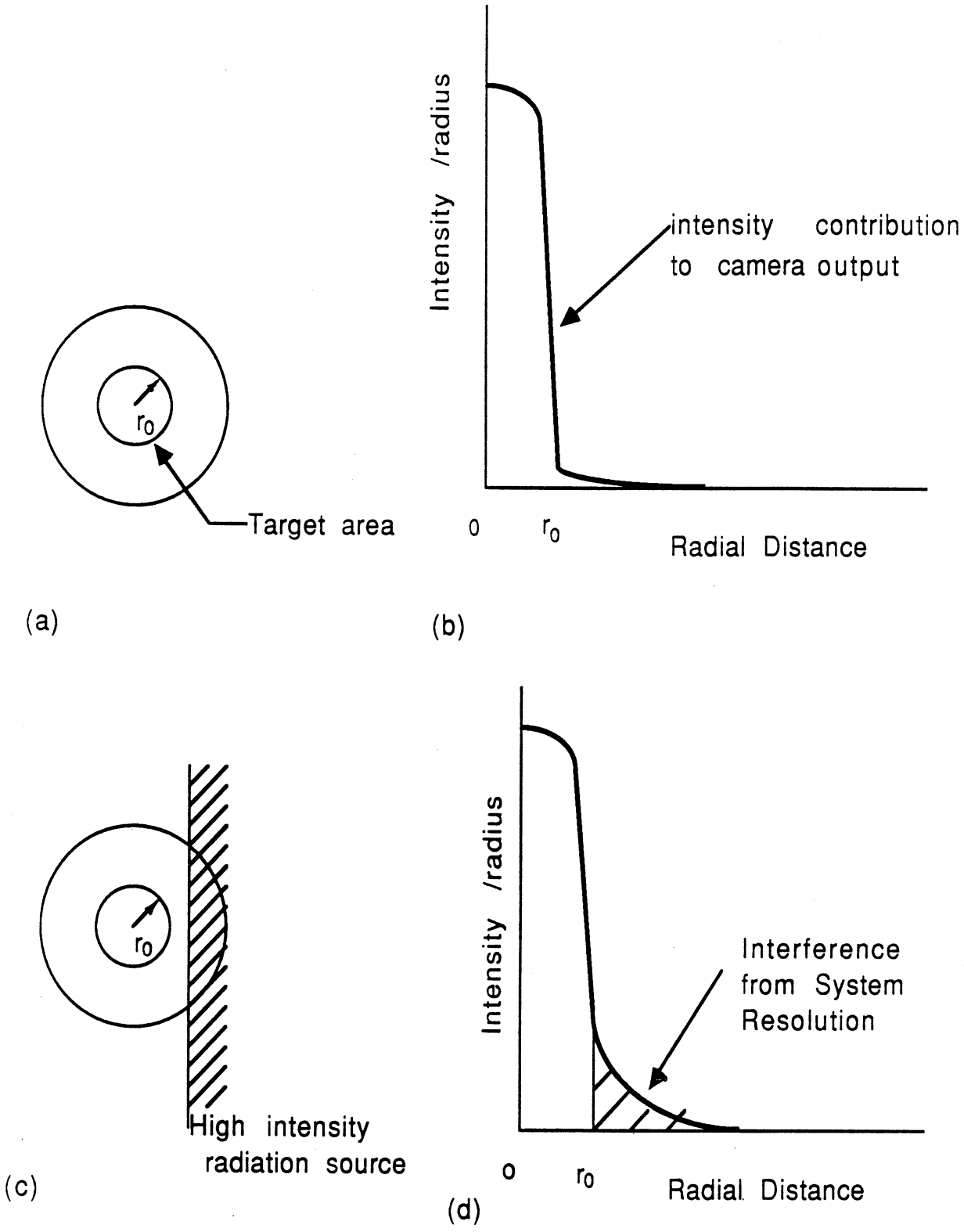

Fig. 20 Interference from system resolution; (a), (b) and (c), (d) : without and with a high intensity heat source near target point respectively

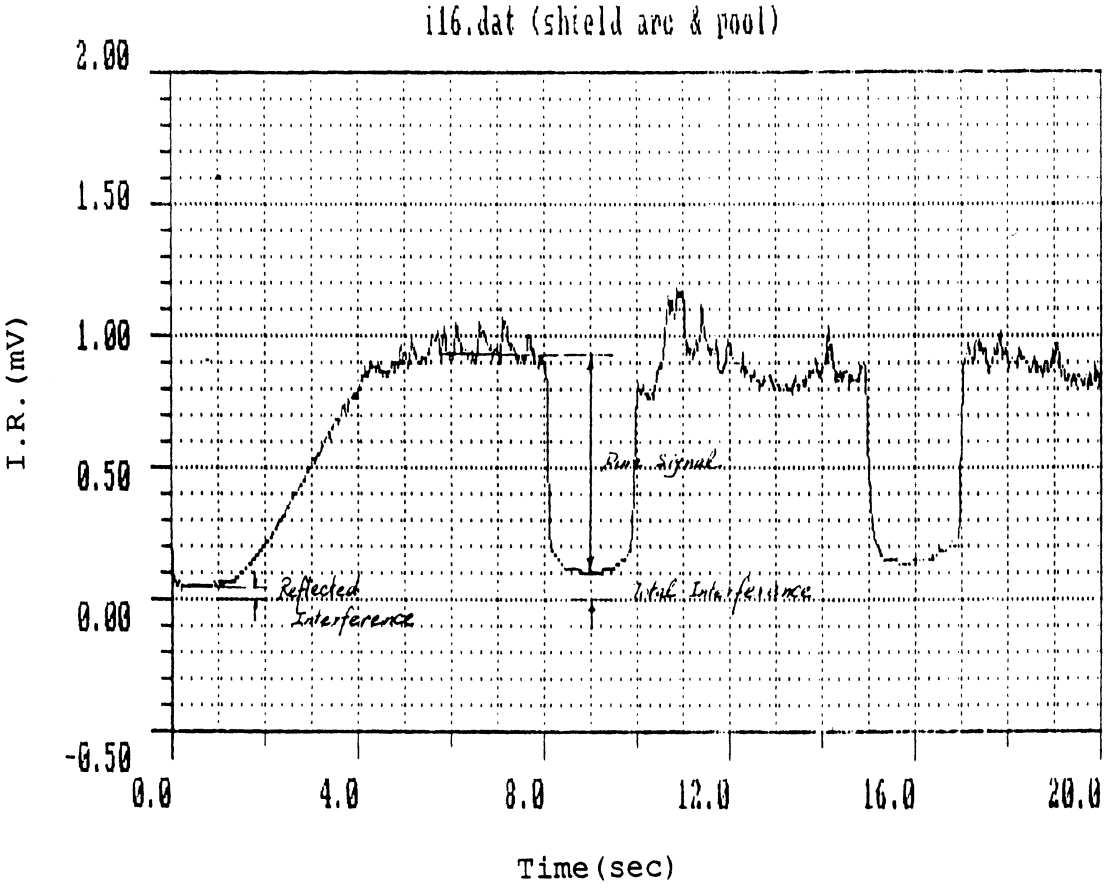

Fig. 21 Plot of interference test data.

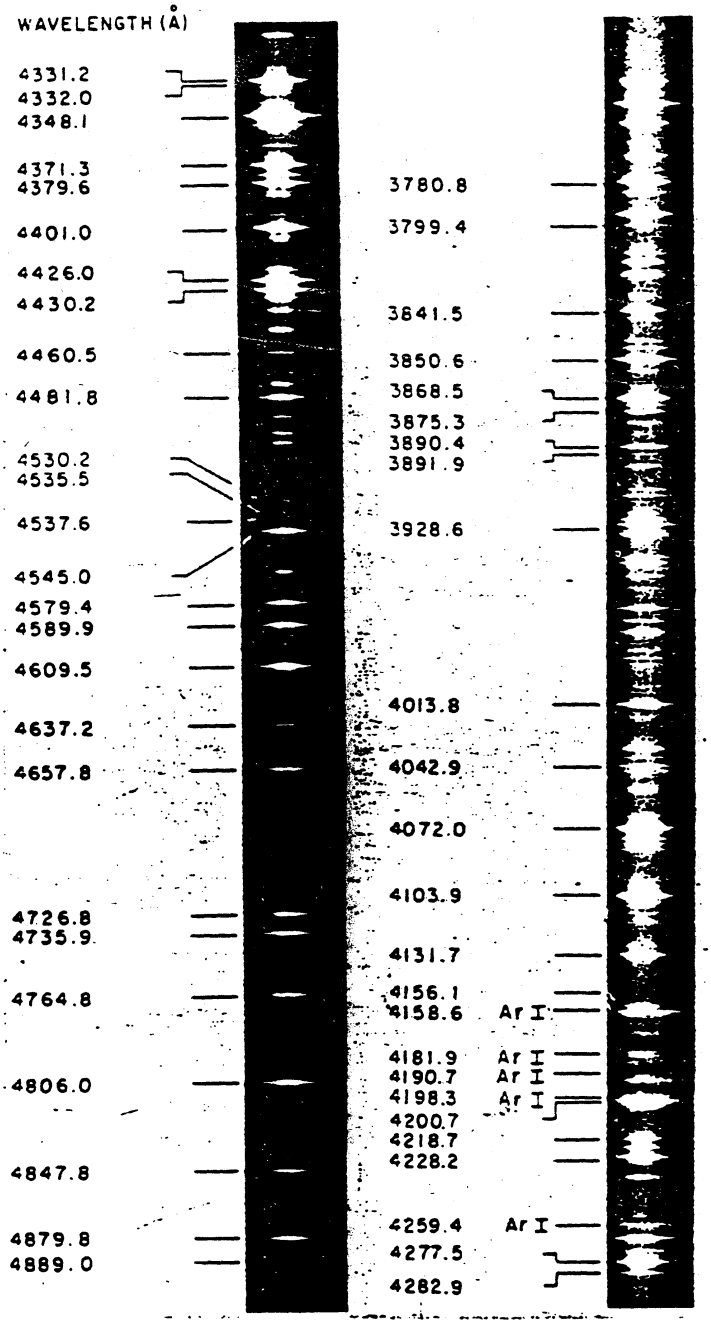

Fig. 22 Spectrum of 100 amp argon arc between 3700 and 4900 $\mathring{A}$ [9]

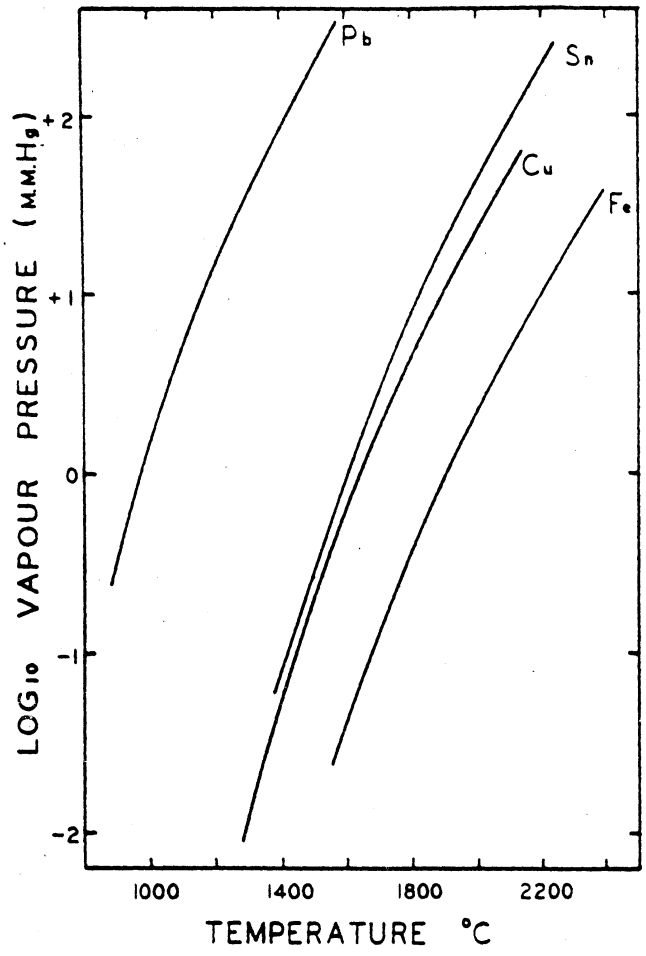

Fig. 23 Vapor pressure vs. temperature of metals.